Growth and Optical Monitoring of Organometallic Vapor Phase Epitaxy

by
Lawrence J. Foley

B.S. Materials Science and Engineering
Massachusetts Institute of Technology, 1993

Submitted to the Department of Materials Science and Engineering in Partial Fulfillment of the Requirements for the Degree of

MASTER OF SCIENCE
in Materials Science and Engineering
at the

Massachusetts Institute of Technology
February 1996

© Lawrence J. Foley. All rights reserved.

The author hereby grants to MIT permission to reproduce and to distribute publicly paper and electronic copies of this thesis document in whole or in part.

Signature of Author . . . .
Department of Materials Science and Engineering
January 19, 1996

Certified by . . . .
Klavs F. Jensen
Professor, Dept. of Chemical Engineering and Dept. of Materials Science
Thesis Advisor

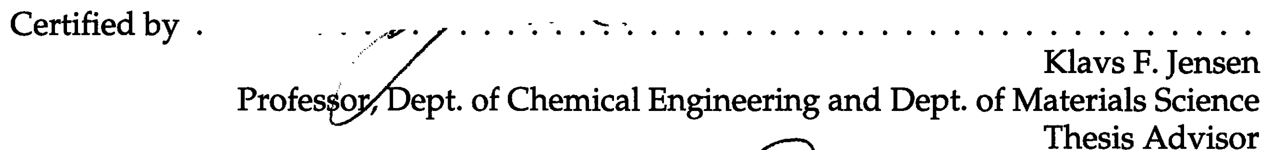

Accepted by . . . .
Michael F. Rubner
TDK Professor of Materials Science and Engineering
Chair, Departmental Committee on Graduate Students

MASSACHUSETTS INSTITUTE
OF TECHNOLOGY

MAR 26 1996

Science

LIBRARIES

Growth and Optical Monitoring of Organometallic Vapor Phase Epitaxy

by

Lawrence J. Foley

Submitted to the Department of Materials Science and Engineering on January 19,1996 in partial fulfillment of the requirements for the Degree of Master of Science in Materials Science and Engineering

Abstract

The OMVPE growth of ZnSe utilizing novel selenium precursors, phosphine selenides, was investigated. Photoluminescence spectra show the epitaxial layers grown to be of high quality. ZnSe films grown at 375 - 425 °C from tripropyl phosphine selenide, TPPSe, and DMZn in a He carrier gas have photoluminescence spectra characterized by strong near band edge emission with very little deep level emission. SEM micrographs demonstrate a good surface morphology with a characteristic "orange peel" texture. Hall measurements of the undoped films show the films to be highly resisitive. SIMS analysis demonstrates low levels of carbon incorporation, $\sim 2 \times 10^{16}$ /cm^3, comparable to levels previously seen. Low levels of H incorporation, $\sim 10^{18}$ /cm^3 are also seen, levels an order of magnitude lower than exhibited by growth with more common Se precursors, indicating the potential use of these phosphine precursors for p-type OMVPE growth applictaions. Due to the low vapor pressure of TPPSe an alternative phosphine selenide, dimethylbutylphosphine selenide, which had an increase of nearly an order of magnitude in the vapor pressure, was examined. SIMS, PL, and SEM analysis demonstrated films that were grown from DMBPSe were comparable to films grown from TPPSe, indicating a similar growth chemistry. Initial studies with a nitrogen doping source, TMSAZ was also investigated. In situ optical monitoring of OMVPE growth was also explored. A laser interferometry technique was utilized to measure the growth rate of ZnSe in situ and was found to be in good agreement with thickness measurements made by SEM. Evaluation of this technique as well as the potential for other characterization will be discussed. Finally, specular reflectance and diffuse scattering of laser light of epitaxial GaSb based films was examined for the potential use of this technique as an in situ monitoring process. Diffuse scattering of incident laser light demonstrates potential for in situ applications to monitor surface morphology and defect orientation.

Thesis Supervisor: Dr. Klavs F. Jensen
Title: Joseph R. Mares Professor of Chemical Engineering and Professor of Materials Science and Engineering

Acknowledgements

There have been many people who have provided valuable help and assistance which has enabled me to perform this research. I would especially like to thank my thesis advisor, Professor Klavs Jensen, without whose support and direction both technical and personal I would not have been able to perform this work. I am also especially appreciative of the support I received from Dr. Christine Wang, my unofficial advisor for the work performed at Lincoln Laboratories. Her knowledge and enthusiasm for her work will be remembered.

There are many others who have also contributed in various ways. I am very appreciative of the entire research group for the many interactions both particular to research and those which were not. I am also appreciative of Michal Danek, a former member of the research group, for his help with the PL measurements and the synthesis of the TPPSe precursor. I would like to thank Jody House for her help with the 10K photoluminescence measurements, Mike Steigerwald at AT&T Bell Laboratories for his synthesis of the assymetrical phosphine source as well as technical discussions of the phosphine selenides, William Rees for the synthesis of the nitrogen doping source that was investigated, and Dr Noble Johnson provided SIMS measurements.

Table of Contents

Abstract 2

Acknowledgements 3

List of Figures 6

1 Introduction

- **1.1 ZnSe Growth** 9
- **1.2 Optical Monitoring Techniques** 10

2 Background

- **2.1 ZnSe Growth History** 12
- **2.2 Proposed Growth System** 15
- **2.3 Optical Monitoring History** 16
- **2.4 ZnSe Interferometry** 17
- **2.5 Specular Reflection and Diffuse Scattering Technique** 20

3 ZnSe Growth

- **3.1 Precursor Synthesis** 21
- **3.2 Vapor Pressure Measurements** 21
  - *3.2.1 Experimental Setup* 21
  - *3.2.2 Vapor Pressure Results* 22
- **3.3 ZnSe Growth Procedure** 25
- **3.4 Film Characterization** 30
- **3.5 Growth Results with TPPSe** 30
  - *3.5.1 Wafer Preparation Techniques* 31
  - *3.5.2 Effect of Wafer Preparation* 31
  - *3.5.3 Effect of Growth Temperature* 33
  - *3.5.4 Effect of VI/II Ratio* 40
  - *3.5.5 H, C and P Incorporation* 43
  - *3.5.6 Effect of Carrier Gas* 46
- **3.6 Growth Results with DMBPSe** 49
- **3.7 Initial Studies of TMSAZ Doping Source** 54

4 Optical Monitoring

4.1 ZnSe Interferometry

4.1.1 Experimental Setup 56

4.1.2 Interferometry Results 56

Growth Rate Mesaurements 56

Surface Morphology 63

Other Uses 63

Limitations 65

4.2 Laser Light Scattering 66

4.2.1 Experimental Setup 66

4.2.2 Specular Reflection 66

Effect of Incidence Angle 68

Effect of Orientation of Defects 71

4.2.3 Diffuse Scattering 71

Effect of Orientation of Defects 73

Limitations 73

5 Conclusions/Recommendations

5.1 ZnSe growth 76

5.2 ZnSe Laser Interferometry 77

5.3 Laser Light Scattering 78

References 79

List Of Figures

2.1 Illustration of laser interferometry 18

3.1 Schematic of experimental setup for vapor pressure measurements 23

3.2 Vapor pressure of TPPSe (●) and DMBPSe (■) at various temperatures. 24

3.3 Schematic of the OMVPE reactor and gas-handling system used for the growth of ZnSe 26

3.4 10K PL spectra of ZnSe. The films were grown at 400 °C with DMZn (5 µmol/min) and TPPSe (5 µmol/min) in He utilizing three wafer preparation techniques: (a) 10 min TPPSe pretreatment, (b) 10 min H_2S pretreatment, and (c) 10 min $(NH_4)_2S$ passivation. 32

3.5 Temperature dependence of the ZnSe growth rate in He from DMZn (5 µmol/min) and TPPSe (5 µmol/min). 34

3.6 SEM micrographs of ZnSe films grown from TPPSe (5 µmol/min) and DMZn (5 µmol/min) in He at (a) 375 °C, (b) 400 °C, (c) 425 °C, and (d) 450 °C. The layer thicknesses were ~0.5 µm (a,b) and ~1.0 µm (c,d). 36

3.7 10K PL spectra of ZnSe. The films were grown from TPPSe (5 µmol/min) and DMZn (5 µmol/min) in He at (a) 375 °C , (b) 400 °C, (c) 425 °C, and (d) 450 °C. 37

3.9 1.9 K near band-edge PL of ZnSe. The films were grown from TPPSe (5 µmol/min) and DMZn (5 µmol/min) in He at various deposition temperatures: (a) 375 °C, (b) 400 °C, (c) 425°C, and (d) 450 °C. 38

3.9 10K PL spectra of ZnSe. The films were grown at 425 °C from TPPSe (5 µmol/min) and DMZn in He at VI/II ratios of (a) 0.5, (b) 1.0 and (c) 2.0. 41

3.10 1.9K near band-edge PL of ZnSe. The films were grown at 425 °C from TPPSe (5 µmol/min) and DMZn in He at VI/II ratios of (a) 0.5, (b) 1.0 and (c) 2.0. 42

3.11 SIMS concentration profiles for (a) hydrogen, (b) carbon, and (c) phosphorous for a ZnSe film grown in He with DMZn (5 μmol/min) and TPPSe (5 μmol/min) at 400 °C (———), and a film grown in H_2 from tBASe (40 μmol/min) and DMZn:NEt_3 (20 μmol/min) at 350 °C (— — —). 44

3.12 10K PL spectra of ZnSe. The films were grown at 425 °C from DMZn (5 μmol/min) and TPPSe (5 μmol/min) in (a) He and (b) H_2. Also shown is a more detailed spectra of the near band edge of the sample grown in H_2. 47

3.13 SIMS concentration profiles for (a) hydrogen, (b) carbon and (c) phosphorous for ZnSe films grown from TPPSe (5 μmol/min) and DMZn (5 mmol/min) at 425 °C in He (— — —) and H2 (———). 48

3.14 SEM micrographs of ZnSe films grown at 425 °C in He from DMZn (5 μmol/min) and (a) TPPSe and (b) DMBPSe, each 5 μmol/min; (c) Comparison of growth rates of ZnSe films grown in He from DMZn (5 μmol/min) and TPPSe (▲) and DMBPSe (O), each 5 μmol/min. 51

3.15 10K PL spectra of ZnSe. The films were grown at 425 °C in He from DMZn (5 μmol/min) with (a) TPPSe and (b) DMBPSe, each 5 μmol/min. 52

3.16 SIMS concentration profiles for (a) hydrogen, (b) carbon, and (c) phosphorous for ZnSe films grown in He with DMZn (5 μmol/min) and TPPSe (———) at 400 °C and DMBPSe (— — —) at 425 °C, each 5 μmol/min. 53

3.17 10K PL spectraof ZnSe. The films were grown at 400 °C in He from DMZn (5 μmol/min) and TPPSe (5 μmol/min); (a) undoped and (b) TMSAZ doped (5×10^{-3} μmol/min). 55

4.1 Schematic of in situ laser interferometry setup 57

4.2 Typical laser interferometry ouput and an SEM image of the cleaved edge of a ZnSe film grown on a GaAs substrate. The interferometry output is a measure of light intensity (mV) as a function of time. Each period represents 0.109 mm growth of the epilayer 58

4.3 Comparison of in situ laser interferometry thickness measurement with SEM measurement of the thickness of the epilayer of a cleaved sample for various ZnSe films. 59

4.4 Comparison of ZnSe growth rates measured during a single growth experiment (———) and individual growth experiments (O). All growth experiments were in He with TPPSe (5 μmol/min) and DMZn (5 μmol/min). 62

4.5 Laser interferometry output of ZnSe films of varying surface morphology. The output is light intensity as a function of time. The inset is an SEM micrograph of the films. 64

4.6 Schematic of experimental setup for laser light scattering for (a) specular reflection and (b) diffuse scattering. 67

4.7 Variation of specular beam intensity as a function of angle of incidence for four InGaAsSb films of vaying surface morphology. Images of the four films can be seen in Figure 4.8. 69

4.8 Normarski phase contrast images of the four InGaAsSb films investigated in Figure 4.7. The images were taken at a magnification of 1600X. 70

4.9 Variation of specular beam intensity as a function of the orientation of the surface morphology for two GaSb films. The images are Normarski phase contrast images of the surface morphology, with the arrow indicating the intial incidence (Rotation = 0) of the laser beam. 72

4.10 Diffuse scattering as a function of orientation for GaSb films of varying surface morphology. The arrow indicates the initial position of the incident light (Rotation=0) with respect to the surface morphology. The Normarski phase contrast images represent a magnification of 1600X. 74

1 Introduction

1.1 ZnSe Growth

The II-VI compound semiconductor family was initially investigated in the 1960's and 70's. The family spanned the wavelength spectrum from the infrared region to the ultraviolet region. With direct bandgaps, high carrier mobilities, and efficient recombination transitions, this class of compound semiconductors showed promise for a variety of optoelectronic devices. However, many problems were encountered with the structural and electronic quality of these materials. Control over the doping was a significant problem, along with the presence of native defects, which served to compensate the layers as well as degrade the overall structural quality. As a result of these problems, and the inability to overcome them with the growth processes available at the time, study of these materials waned.

There was a renewed interest in this class of materials beginning in the early 1980's. With the maturation of new non equilibrium growth techniques, namely molecular beam epitaxy (MBE) and organometallic vapor phase epitaxy (OMVPE), it was believed that some of the problems that were initially encountered could be overcome by the advances in these growth processes.

ZnSe is a II-VI compound semiconductor with a direct band gap of approximately 2.67 eV at room temperature. These properties make it an ideal candidate for blue to blue-green LED and laser applications, such as optical memory and thin film display materials. The most immediate impact of ZnSe based laser devices is believed to be in the optical storage area, where the decrease in wavelength of

nearly a factor of two over existing devices is expected to yield nearly a fourfold increase in optical storage densities.

Organometallic vapor phase epitaxy (OMVPE) is a non equilibrium growth technique in which the precursors are delivered in the gas phase, at least one of which is an organometallic compound. Since the process is a non equilibrium technique, it has the advantage of much lower growth temperatures than equilibrium growth processes such as liquid phase epitaxy. This is a very important distinction for the growth of ZnSe and other II-VI compound semiconductors. Due to the large band gaps, an effect owing to the relatively large ionicity of the bonding, the formation of native defects and self compensation are significant problems, becoming increasingly important as the growth temperature is increased. The reduction of growth temperature by non equilibrium techniques such as OMVPE and MBE is therefore critical for growing device quality epilayers.

While significant progress has been made in the molecular beam epitaxy of ZnSe films, this has not been mirrored by the OMVPE process. The use of novel phosphine selenide precursors to address some of the p-type doping problems will be a focal point of this thesis. Some of the specific problems encountered in the OMVPE growth of ZnSe and the particular motivation of this research will be addressed in the following chapter.

1.2 Optical Monitoring Techniques

As the demands placed upon the growth of epitaxial films become increasingly stringent, the ability to monitor the growth process in situ becomes vital to the ability to meet these new requirements. In situ monitoring of the MBE process has been one of the significant advantages that MBE holds over OMVPE growth. Since the growth in the MBE process takes place under ultra high vacuum conditions, the ability to use

electron monitoring techniques, such as reflection high energy electron diffraction (RHEED), has allowed detailed analysis of the surface structure during the growth process. The RHEED technique has also been utilized as an in situ tool for thickness and compositional calibration, as well as real time control, which has been crucial to the growth of reproducible device structures. [1] However, OMVPE growth takes place at much higher pressures, which precludes the use of some of the techniques that are available to MBE. Much of the characterization to date relies on ex-situ techniques, which makes it more difficult to get a clear picture of the growth processes or some of the problems that may occur during the growth.

Recently, monitoring techniques utilizing visible light have received attention for in situ OMVPE applications. Since the growth environment is normally transparent to visible light, optical techniques have the potential to provide a much more detailed picture of the growth process. Therefore the other objective of this thesis is the study of the use of a laser interferometry technique to monitor the growth of ZnSe in situ, and an investigation of laser reflection and scattering techniques that may be employed for other materials systems.

2 Background

2.1 ZnSe Growth History

Specific interest in ZnSe based devices arose from the direct band gap of 2.67 eV at room temperature which lies in the blue to blue green portion of the visible spectrum. These qualities make it a strong candidate for numerous optoelectronic devices, including LED's and lasers for thin film display applications and optical storage devices.

Similar to many other II-VI compound semiconductors one of the major stumbling blocks to the development of ZnSe based devices has been the inability to dope the semiconductor both n-type and p-type. The problems of self-compensation and formation of native defects directed the research to non equilibrium growth techniques. While the growth of good n-type ZnSe material has been demonstrated by both OMVPE and MBE [2], it has been far more difficult to make progress with the p-type layers. Recently, advances in the molecular beam epitaxy of p-type material have been made, and devices such as lasers have been demonstrated. [3-6] However, similar progress in the OMVPE growth of p-type ZnSe has not been seen. The desire to reduce native defect formation by lowering the deposition temperature and problems with impurity incorporation has lead to the investigation of numerous precursors.

A variety of selenium precursors have been studied for the OMVPE growth of ZnSe. Many of the initial studies utilized hydrogen selenide, H_2Se [7-9], a precursor which had the benefit of low growth temperatures, ~280 °C, as well as an ability to deliver high concentrations in the gas phase. However, the use of H_2Se has several

disadvantages. It is prone to premature reactions in the gas phase which degrades the quality of the film and it is also highly toxic. Dimethyl and diethyl selenides [7,10,11] were investigated as potential replacements for H_2Se, however the high growth temperatures, >500 ^oC, lead to the problems of increased native defect formation.

The motivation to drive down the deposition temperatures lead to the study of Se based alkyls with large organic groups. This was similar to the strategy employed with Te based alkyls in the growth of ZnTe. [12] The increased number of organic groups leads to a lower decomposition temperature, and thus lower growth temperatures. Studies with methylallylselenide, however, did not reduce the growth temperature and additionally, there were problems with increased levels of carbon incorporation in the ZnSe films. While carbon impurities have been found not to affect the electrical or optical properties of ZnSe, elevated concentrations are expected to degrade the overall structural quality of the film and affect lifetime of potential devices. Ditertiarybutyl selenide, DTBSe, was found to grow high quality ZnSe layers at relatively low growth temperatures (~330^oC), however impurity incorporation in the films was once again found to be a significant problem. [13] The Cl contamination in the films was believed to originate from impurities in the precursor. This problem probably could be overcome by improved purification techniques, but questions of hydrogen and carbon incorporation still remained.

N-type ZnSe layers have been grown utilizing a variety of group III and group VII dopant atoms. Elements from group III, which substitute on the Zn site, include Ga and Al. The use of these dopant atoms have been reported for both MBE and OMVPE growth with doping levels of approximately $10^{17}/cm^3$. [15,16] The halogen group elements have also been demonstrated to be good donor atoms, substituting on the Se site. Excellent control over the doping level as well as stability has been demonstrated for ZnSe films grown with Cl [17] and I [18] dopant atoms. The development of ZnSe devices has not been hindered by ability to grow n-type layers; one of the major problems has been the inability to achieve high quality p-type layers and that has retarded the development of ZnSe based devices.

Elements investigated for p-type applications include those from group Ia (Li, Na) for substitution on the zinc site, and elements from group Va (N, P ,As) for substitution on the selenium site. The light alkali elements, Li and Na, have been the most researched of the group I elements. While the solubility of both of these atoms is high enough for doping applications, several problems have been encountered. Quality p-type layers with hole concentrations up to $\sim 10^{17}/cm^3$ have been demonstrated for Li, with a shallow acceptor level of 124 meV. [19] However, attempts to push the incorporation levels higher has lead to the Li atoms going into the lattice interstitially, and behaving as n-type dopants. [20] A further problem with lithium is the relatively high mobility of the atom in ZnSe at normal processing temperatures. This may lead to problems of maintaining dopant level control and uniformity. P-type ZnSe grown using Na dopant atoms have encountered similar problems. At low concentrations, Na is a shallow acceptor at 134 meV [21], however at higher concentrations the dopant atom again incorporates interstitially.

The group Va elements show promise since the size of the atoms is similar to the Se atom and the solubility of the elements appears to be high enough for device applications. The use of phosphorous atoms as an acceptor in ZnSe has lead to significant problems. At levels up to $\sim 10^{16}$ $/cm^3$, phosphorous is a shallow acceptor, however at higher doping levels phosphorous incorporates in deep acceptor states, a behavior which is unsuitable for optical applications. [22]

Nitrogen has been perhaps the most widely studied of the potential p-type dopant atoms. Similarly, most of the light emitting devices that have been demonstrated to date have utilized nitrogen as the p-type dopant. P-type layers grown by MBE have been able to attain relatively high levels of incorporation, $\sim 10^{18}$ $/cm^3$, using a nitrogen plasma. [23] These results have not been matched in the OMVPE growth of ZnSe. Park et al, have demonstrated OMVPE growth of ZnSe with nitrogen incorporation levels of approximately 10^{18} $/cm^3$ [10,24] however electrical measurements of these films reveal that only 10^{15} $/cm^3$ are active. It was speculated

that the nitrogen atoms were incorporating into the films as part of a nitrogen-hydrogen complex where the hydrogen served to passivate the nitrogen dopant atoms. This hypothesis was confirmed by Wolk and Kamata, in FTIR and SIMS studies showing the presence of nitrogen-hydrogen bonds in the N doped films [25,26]. Studies using NH_3 [10], plasma cracked NH_3 [27], and amines [28] as nitrogen dopant sources have all encountered the passivation problem. The problem of hydrogen passivation is not believed to be solely attributed to the presence of H radicals coming from the dopant source, the Se and Zn precursors are also potential donors of active hydrogen radicals. Many of the common selenium precursors utilized, such as H_2Se, RSeH, R_2Se (R=alkyl group) can significantly contribute active hydrogen atoms that can passivate the group Va dopant atoms. Similarly, β-hydride elimination processes from either the Zn or Se precursors can also potentially contribute to the problem. Thus it is believed the ability to grow p-type ZnSe by organometallic vapor phase epitaxy is limited to the ability to eliminate, or at least greatly reduce, the presence of active hydrogen radicals during growth which can originate from either the Zn, Se, or nitrogen dopant precursors .

2.2 Proposed Growth System

The need for alternative selenium precursors that will reduce the contribution of active hydrogen was the underlying motivation for this research. Tri-n-propyl phosphine selenide, TPPSe, $(C_3H_7)_3PSe$ was proposed to help alleviate the active hydrogen problem. Trialkyl phosphines are known to be highly stable in III/V growth systems. [11] Thus it is believed that this precursor will decompose at the phosphorous selenium bond, and that the phosphine would be a stable product. The proposed growth system is as follows:

$$\text{TPPSe} + \text{DMZn} \longrightarrow \text{ZnSe} + \text{TPP} + CH_4$$

An inert carrier gas, He, was chosen in order to avoid any carrier gas interactions with the growth, however the use of H_2 carrier gas was also investigated. Dimethyl zinc, DMZn, was chosen as the zinc source. Although diethyl zinc is also a commonly used source, it was believed that the DEZn may contribute to the problem of hydrogen incorporation through β-hydride elimination processes. Due to the relatively low vapor pressure of the TPPSe source, as will be seen in the subsequent chapters, an alternative asymmetrical phosphine, dimethylbutyl phosphine, was also investigated in the hopes of increasing the volatility of the selenium precursor. Finally, initial studies of a potential doping source, $Zn\{N[Si(CH_3)_3]_2\}_2$ (bis[bis(trimethylsilyl)amido] zinc; TMSAZ), were performed. This compound was chosen since it is believed to split at the nitrogen-silicon bonds, and the resulting Zn-N bonds will serve to preferentially place the nitrogen substitutionally on the Se site. More traditional precursors, such as NH_3 were not investigated, since as described in the previous section, N-H complexes were shown to lead to electrically inactive p-type material.

2.3 Optical Monitoring History

As mentioned previously, the need for in situ monitoring of the OMVPE process has recently lead to an increased investigation of optical techniques. The use of visible light has several advantages which lends itself to the OMVPE process. It is a non-destructive process and is transparent to most OMVPE growth environments.

The optical techniques that are available and have been explored for some materials systems include reflectance [29-33], scattering [34], ellipsometry [35] and interferometry techniques [36]. These techniques vary in both their complexity and compatibility to existing OMVPE processes. Furthermore, the type and amount of information that can be derived from these techniques similarly varies. Information on the surface morphology and defects, growth rate and thicknesses, optical constants, and the growth process have been gathered through the various techniques mentioned.

However, due to issue of compatibility to the reactor, as well as the materials system being investigated, not all of these techniques can be utilized for a specific area of research. Some of the issues concerning the implementation of these techniques will become more clear in the following sections.

2.4 ZnSe Interferometry

The ZnSe films discussed in this thesis were grown on GaAs substrates. Since the bandgap of ZnSe is on the blue edge of the visible light spectrum, the film is transparent to the 632.8 nm radiation that was used, whereas GaAs, with a bandgap of approximately 1.42 eV, is not. An illustration of the incident laser beam on the sample is shown in Figure 2.1. The laser beam travels from the air through the ZnSe film and into the substrate. Depending on the difference between the distances light travels from the air/ZnSe interface and the ZnSe/GaAs interface, there will be varying degrees of constructive and destructive interference. It can easily be seen from the figure that the optical pathlength difference is a function of the film thickness. Thus the film thickness can be monitored in situ by monitoring the interference cycles.

The reflectance coefficient of the sample is determined by the following equations, for a laser beam that is polarized in the direction perpendicular to propagation:

$$r = E^r / E^i = (r_1 + r_2 e^{-2\beta i}) / (1 + r_1 r_2 e^{-2\beta i}) \tag{2.1}$$

where E^r and E^i are the magnitudes of the electric field of the reflected and incident beams. β, r_1,r_2 are defined as:

$$\beta = 2 \pi d n_1 \cos \phi_1 / \lambda$$

$$= 2 \pi d (n_1^2 - \sin^2\phi_0)^{1/2} / \lambda \tag{2.2}$$

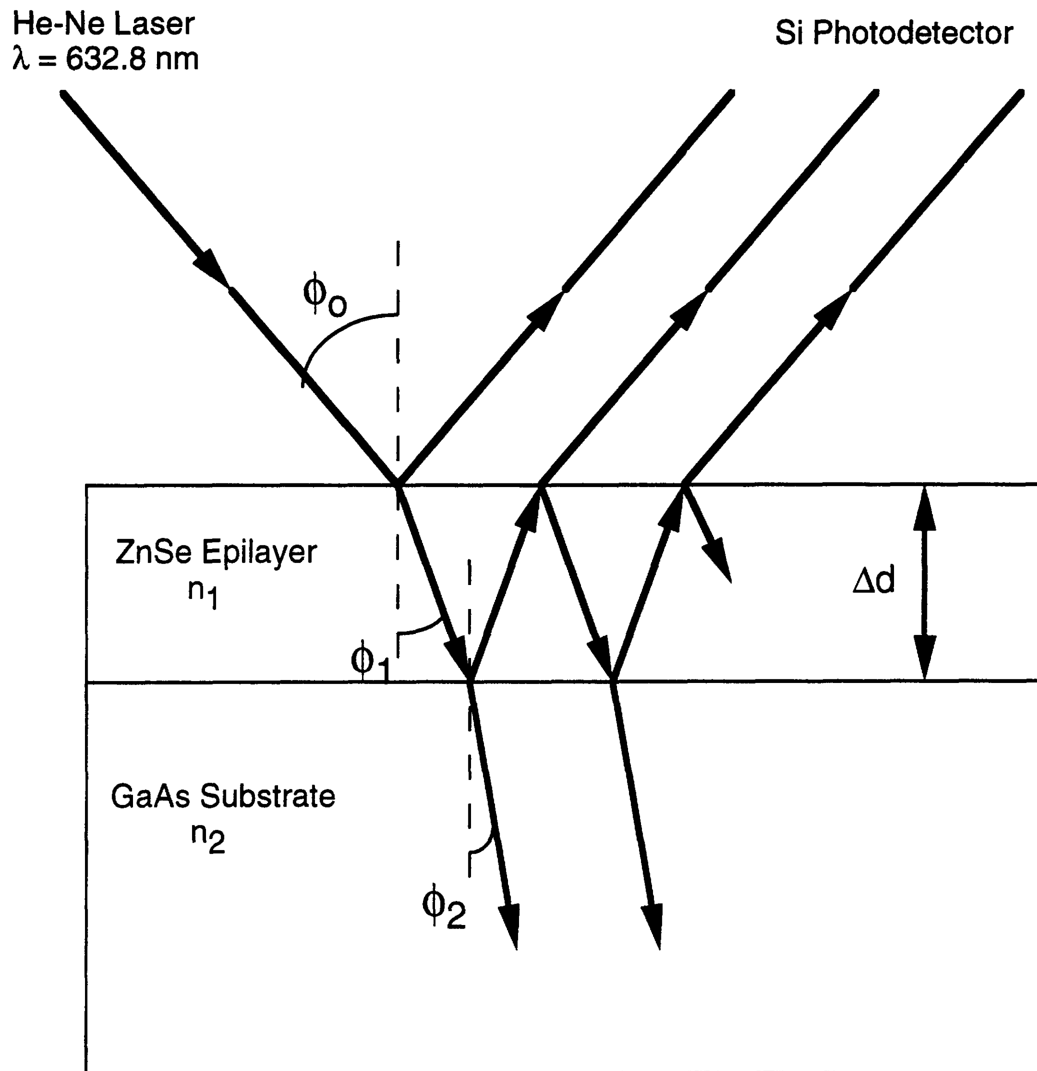

Figure 2.1: Illustration of laser interferometry.

$$r_1 = (\cos \phi_0 - n_1 \cos \phi_1) / (\cos \phi_0 + n_1 \cos \phi_1) \quad (2.3)$$

$$r_2 = (n_1 \cos \phi_1 - n_2 \cos \phi_2) / (n_1 \cos \phi_1 + n_2 \cos \phi_2) \quad (2.4)$$

where n_1 and n_2 are the indices of refraction of the ZnSe epitaxial layer and the GaAs substrate, d is the thickness of the film, λ the wavelength of the incident radiation and ϕ_0 , ϕ_1 , ϕ_2 are the angles defined in Figure 2.1. The reflectance, $\mathcal{R}$,is determined by

$$\mathcal{R} = r^* \, r \quad (2.5)$$

The period of the reflectivity is $\beta = n_1 \pi$. Thus the cycle between constructive (or destructive) interference is related to the change in film thickness, Δd, by:

$$\Delta d = \lambda / 2 (n_1^2 - \sin^2\phi)^{1/2} \quad (2.6)$$

For the particular experimental setup utilized in this thesis, the laser light is incident normal to the substrate, so equation 2.6 simplifies to:

$$\Delta d = \lambda / 2 n_1 \quad (2.7)$$

where once again Δd is the change in film thickness, λ the wavelength of the incident light, and n_1 the index of refraction of the ZnSe epilayer grown. In order to determine the growth rate, the thickness grown is divided by the time of one period, τ:

$$\text{growth rate} = \Delta d / \tau = \lambda / 2 n_1 \tau \quad (2.8)$$

Since scattering by the film will affect the overall intensity of light that is collected, some information on the surface morphology of the film can be also be

obtained from this technique. One of the major limitations of the use of interferometry is the compatibility of the technique to the materials system being investigated; the epitaxial material grown must be transparent to the radiation, while the substrate is not. Smaller bandgap materials will not be able to utilize this technique unless very long wavelength lasers and detectors are used and the films are grown on even smaller bandgap substrate material. For systems such as GaSb, other techniques need to be developed.

2.5 Specular Reflectance and Diffuse Scattering Techniques

Laser light scattering (LLS) is a surface probe technique that relies on the incident light being scattered by imperfections on the surface of the sample. It offers the advantage of being the optical monitoring technique with the least experimental complexity. It simply requires an intense source of light and a detector. One can monitor the reflected beam (specular reflectance) or the light that it is scattered nonspecularly, referred to as diffuse scattering in this thesis. Information on the surface morphology and defects can be obtained from these techniques.

Horikoshi et al, have utilized LLS to detect the onset of defect formation on (001) GaAs growth. [37] Pidduck et al, have utilized this technique to monitor step flow on surfaces. [38,39] Use of the LLS technique to monitor GaSb and other Sb based compound semiconductors will be investigated in this thesis. This technique was chosen because of its relative experimental simplicity and potential compatibility with the OMVPE reactor available. An assessment of the potential of this technique and the sensitivity and type of information obtained by this technique will be addressed.

3 ZnSe Growth

3.1 Precursor Synthesis

The tri-n-propyl phosphine selenide was synthesized in a nitrogen glove box using tri-n-propyl phosphine (Aldrich chemicals) and elemental selenium shots (Aesar). These were mixed and heated in a quartz vessel using a slight excess of phosphine to insure that all of the selenium would be consumed. The resulting compound was then transferred into a glass bubbler and installed on the OMVPE system. A more detailed description of the synthesis is given elsewhere. [40] The asymmetrical phosphine selenide, dimethyl(butyl) phosphine selenide was synthesized by a similar procedure by Dr. Mike Steigerwald at AT&T Bell Laboratories. The bis[bis(trimethylsilyl)amido] zinc doping source, TMSAZ, was synthesized by Dr. Bill Rees at Georgia Tech University. [41]

3.2 Vapor Pressure Measurements

3.2.1 Experimental Setup

It was necessary to measure the vapor pressure of these new phosphine selenide compounds in order to establish the appropriate delivery of the precursors to the

reactor. The measurement was performed with the bubbler installed on a high vacuum system which contained a 10 Torr baratron (MKS) to directly measure the vapor pressure. A schematic of the experimental setup is shown in Figure 3.1.

The measurement was performed by first evacuating the section of tubing using a turbomolecular pump. The tubing was then isolated and the bubbler opened. The bubbler was typically left open for 15-20 minutes, and the vapor pressure was monitored until steady state was achieved and the final reading was taken. The bubbler was then closed, the line evacuated, and the process repeated. The measurements were performed over a range of temperatures, with several measurements made at each temperature to check for consistency. The sources were heated by a temperature controlled bath and the lines were wrapped and heated to approximately 5 degrees above the sampling temperature to avoid condensation of the vapor on the stainless steel lines. The vapor pressure measurements also served to completely degas the samples and insured that any higher volatility compounds were removed from the bubbler prior to the ZnSe growth experiments.

3.2.2 Vapor Pressure Results

The vapor pressures of tripropyl phosphine selenide, TPPSe, and dimethyl(butyl) phosphine selenide, DMBPSe, are plotted in Figure 3.2. TPPSe has a melting point of 32 ^{o}C and the vapor pressure in the range of 40-90 ^{o}C is found to fit the following equation:

$$\ln P = -3423 / T + 8.496 \qquad (3.1)$$

where P is the vapor pressure of the source in Torr, and T is the temperature of the source in Kelvin. The vapor pressure of TPPSe is found to range from about 5 mTorr at 40 ^{o}C to approximately 100 mTorr at 90 ^{o}C, which is relatively low for typical delivery of gas phase precursors. It was therefore necessary to keep the source and the delivery lines at elevated temperatures to deliver an appropriate amount of the compound

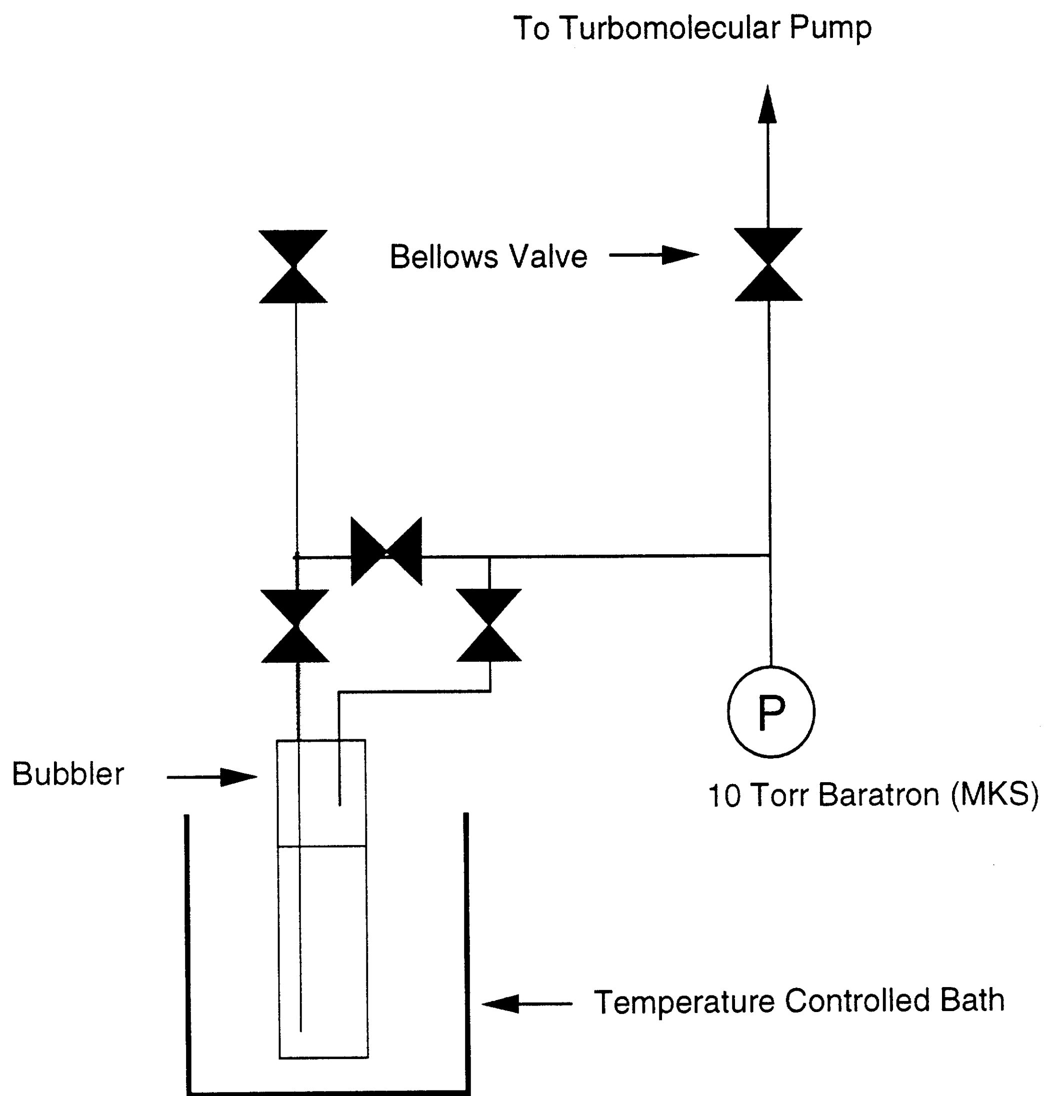

Figure 3.1: Schematic of experimental setup for vapor pressure measurements.

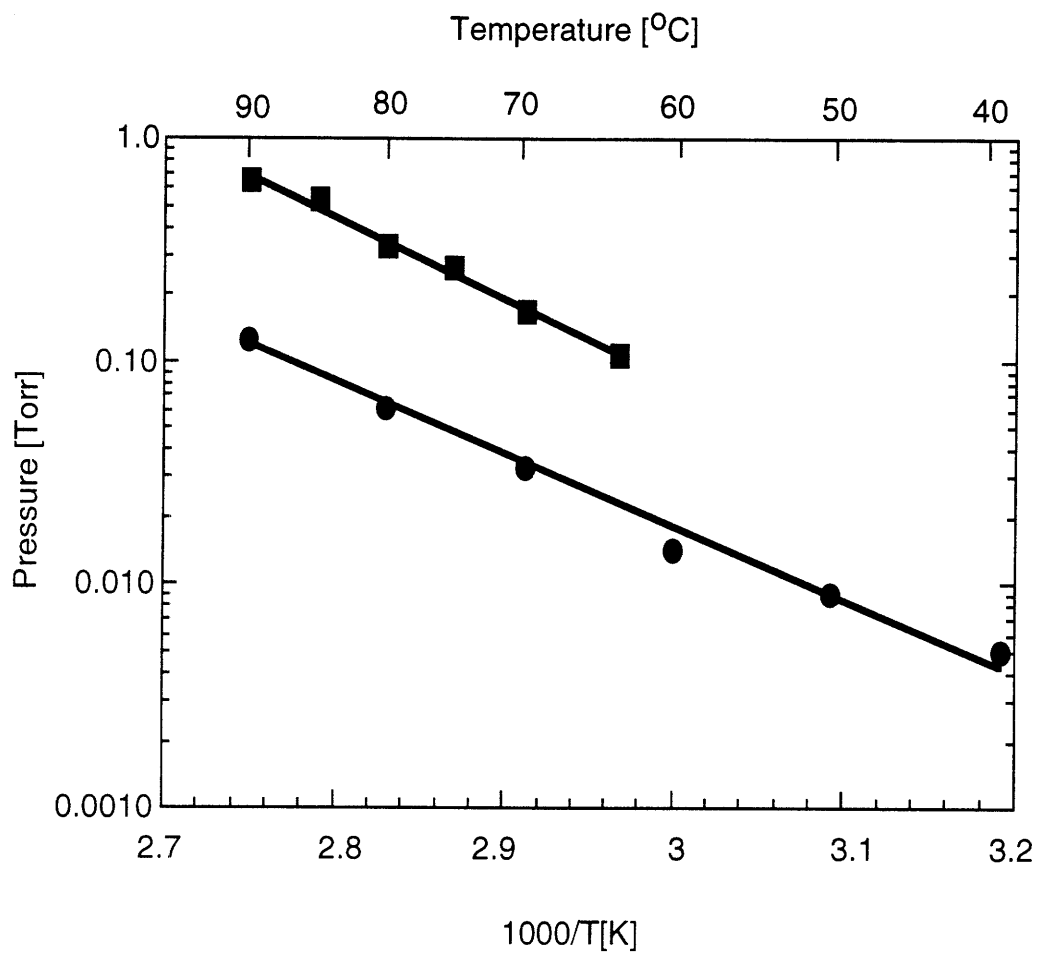

Figure 3.2: Vapor pressure of TPPSe (●) and DMBPSe (■) at various temperatures.

The low volatility of this compound makes it unsuitable for commercial OMVPE compound semiconductor applications. The search for a more volatile source led to the study of DMBPSe. Due to the asymmetrical nature of the phosphine group it was theorized to have a higher vapor pressure than TPPSe. As evidenced by Fig 3.2, this is indeed the case, with an increase of nearly an order of magnitude in the vapor pressure. The melting point of this compound was 58 °C and the vapor pressure in the range of 60-90 °C was found to fit the following equation:

$$\ln P = -3680 / T + 9.959 \qquad (3.2)$$

While there was a marked improvement in the vapor pressure, it was still necessary to keep this source at elevated temperatures. Despite this compound also not being suitable for typical applications, it proved useful in confirming the viability of the trialkyl phosphine growth chemistry. Furthermore, the study of DMBPSe demonstrates the potential to develop more volatile phosphine precursors.

The vapor pressure of the TMSAZ doping source has been previously determined [42]:

$$\ln P = -10630 / T + 29.65 \qquad (3.3)$$

Vapor pressure measurements were made at two temperatures to confirm these results. Once again, due to the low volatility of the compound, it was necessary to keep the source above room temperature.

3.3 ZnSe Growth Procedure

The ZnSe film growth was performed in a vertical downward flow OMVPE reactor. A schematic of the reactor and the gas handling system is illustrated in Figure 3.3. For all of the ZnSe growth experiments the reactor pressure was held at 300 Torr with a total flow rate of carrier gas through the reactor of 1 liter/min. Ultra high purity

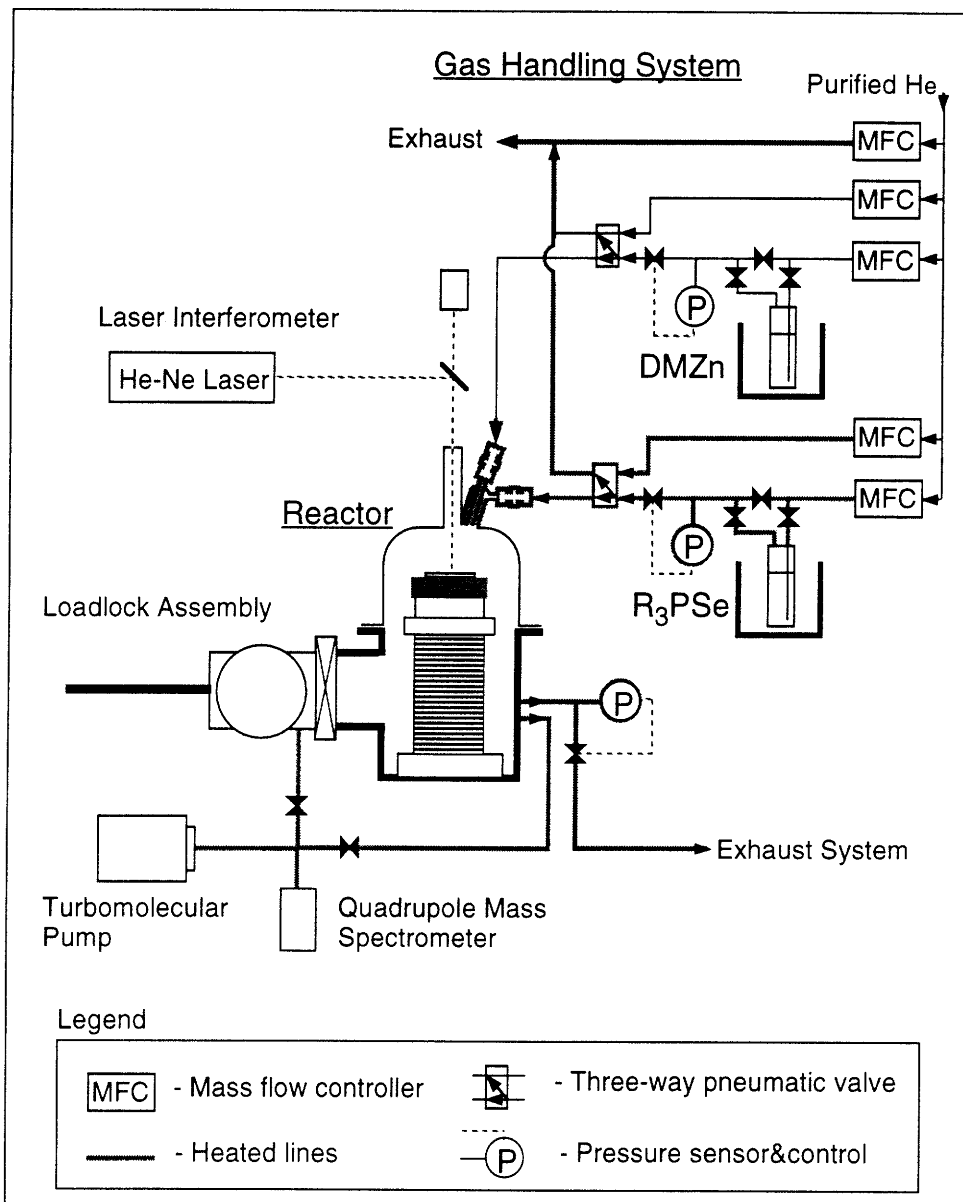

Figure 3.3: Schematic of the OMVPE reactor and gas-handling system used for the growth of ZnSe.

helium (Matheson Gas) was typically used, however ultra high purity hydrogen gas (Matheson Gas) was also utilized to investigate the effect of the carrier gas.

The ZnSe epitaxy was performed on (100) GaAs substrates. The preparation of the substrates and the effect on the ZnSe films will be detailed in the following section. After the wafers were cleaned, they were placed on a molybdenum susceptor and loaded into the load lock chamber. The chamber was evacuated to approximately 10^{-6} Torr, backfilled with He to 600 Torr and transferred to the growth chamber by a magnetically coupled arm. The growth chamber was then purged with the particular carrier gas and the exhaust was monitored with a mass spectrometer for the presence of any contaminants. Typically, a signal indicating a residual water level of approximately 5×10^{-9} was the only contaminant observed.

The molybdenum susceptor was heated resistively, and a calibration experiment comparing the temperature controller to the temperature of a thermocouple that was cemented onto the surface of a GaAs wafer was performed prior to the set of growth experiments. Growth experiments were performed on a 1 cm^2 GaAs sample which was placed in the center of the susceptor.

A similar growth procedure was maintained for all of the growth experiments, in order to prevent any potential variance in the growth results. The organometallic bubblers were opened 30 minutes prior to the start of the growth. The carrier gas flows, as well as the reactor and bubbler pressures were all stabilized 1 hour prior to the growth. The selenium precursor was diverted into the growth chamber once it was opened, while the DMZn source flowed to the exhaust line. Following the particular pretreatment of the substrate, which will be outlined in the following section, the susceptor was ramped to the appropriate deposition temperature. Growth was initiated by switching the DMZn source into the reactor with a three-way pneumatic valve. The flow rates, pressures, and susceptor and bubbler temperatures were all

monitored during the growth, to insure constant growth conditions. Growth was terminated by switching the Zn source to the exhaust line. The temperature of the susceptor was ramped down and the Se source was then diverted to the exhaust. The reactor was purged for at least 1 hour before transferring the sample from the growth chamber to the load lock and the sample was removed.

Dimethyl zinc (Air Products) was used as the Zn source in all of the experiments and the bubbler was held at -20 °C, with typical flow rates ranging from 2-10 sccm. The pressure over the bubbler was typically held at 960 Torr, which resulted in delivery rates of 2.5-7.5 μmol/min according to the following equation:

$$P = (VP)(F) / 22400(\mu) + VP \tag{3.4}$$

where P is the pressure in the bubbler, VP is the vapor pressure of the source, F is the flow of carrier gas through the bubbler (in sccm) and μ is delivery rate of the source (μmol/min).

The tripropyl phosphine selenide source was held at 90 °C owing to the relatively low volatility of the source demonstrated in Figure 3.2. It was therefore necessary to heat all of the Se delivery lines to avoid condensation, as well as the exhaust lines to prevent any possible clogging. The lines were wrapped with heating tape and heated to 120-140 °C. Typical flow rates through the Se bubbler were on the order of 150 sccm, with the pressure in the bubbler equal to the reactor pressure of 300 Torr. This resulted in Se delivery rates ranging from 2.5-7.5 μmol/min. The dimethyl(butyl) phosphine selenide source was held at 60 °C, with a pressure in the bubbler of 300 Torr. With flow rates of approximately 120 sccm, the delivery rate of the DMBPSe was varied from 2.5 - 7.5 μmol/min. The delivery lines for the DMBPSe were heated to 80 -90 °C to prevent condensation.

For the doping investigations, the TMSAZ source was held at 50 °C and was mixed with the DMZn vapor before entering the reactor. Once again the delivery lines were wrapped with heating tape and heated to approximately 60-70 °C to avoid any condensation problems. The pressure in the bubbler was 900 Torr and with flow rates of approximately 5 sccm through the bubbler, the delivery rate was approximately 5×10^{-3} μmol/min.

The quartz housing of the reactor was cleaned periodically, depending on the amount of wall deposit. Typically deposits were seen at the level of the susceptor and below, there was rarely any deposit visible at the inlet to the reactor where the gases mixed. The housing was cleaned with concentrated nitric acid and, if necessary, hydrofluoric acid. This was followed by a thorough rinse with deionized water and the reactor was then placed in an oven at 150 °C. After reinstalling the quartz housing the growth chamber was pumped down to approximately 10^{-6} Torr and leak checked with He utilizing the mass spectrometer installed on the system. This procedure was followed by a purge in the He carrier gas for at least 24 hours. Care was taken in determining the order of experiments; the reactor was not cleaned in the middle of a series of runs investigating a particular variable. Similarly, experiments that might be expected to lead to significant wall deposit, for example a high growth temperature or growth in H_2 carrier gas, were performed last in the series of runs, so that the reactor would not have to be opened and cleaned until the series was complete.

A molybdenum susceptor was utilized for these experiments. The susceptor was cleaned between growth runs using a heated 10 %KOH solution with approximately 10 ml of H_2O_2 added to the 200 ml solution. The susceptor was then thoroughly rinsed with deionized water and baked in an oven at 150 °C.

3.4 Film Characterization

Various film characterization techniques were performed to examine the quality of the epitaxial films. The 10K photoluminescence was examined using the 325 nm line of a He-Cd laser as the excitation source. The light was collected in a 0.5 m spectrometer (Jarell Ash) and a UV lamp with an emission line at 407.4 nm was used for calibration purposes. The characterization was performed utilizing a He cryostat (Janis). The 1.9K PL measurements were performed using a Spex 1404 spectrometer with a 0.85m double monochromator and the 325 nm line of a He-Cd laser at low power densities (~60mW/cm^2). The surface morphology of the films was observed with a Cambridge scanning electron microscope (model 250 Mk3). Hall measurements were made using the four point probe technique, with annealed indium contacts used. Finally, SIMS analysis was performed at Charles Evans & Associates, along with the help of Dr. Noble Johnson at Xerox Corporation. A Cs^+ ion beam (ion current of 53 nA, ion impact energy of 14.5 keV) was used and H, C and P incorporation levels were investigated. A ZnSe film with a known ^2H dose was used for calibration of the hydrogen level. C and P levels were based on calculated sensitivity factors by Charles Evans and Associates.

3.5 Growth Results with TPPSe

The majority of the growth experiments were performed with the TPPSe source. While the DMBPSe source was more volatile, there was a limited supply of this source and TPPSe was relatively easy to synthesize since the tri-n-propyl phosphine was readily available from Aldrich Chemicals. Thus initial studies with TPPSe were performed to determine the feasibility of the new growth chemistry and growth with DMBPSe was performed to confirm the growth results and demonstrate the ability to use alternative trialkyl phosphine selenide precursors.

3.5.1 *Wafer Preparation Techniques*

Semi-insulating and Zn doped (100) GaAs was used as the substrate material for the growth. The wafers were prepared by first degreasing them in heated trichloroethylene for 10 minutes followed by heated acetone for 10 minutes. The wafers were then placed in concentrated H_2SO_4 for 30 seconds. At this point a couple of preparation methods were investigated. Since GaAs is known to develop a soft oxide on the surface when exposed to air, several techniques were explored to either passivate the surface to prevent the oxide from forming, or to strip the soft oxide with a pretreatment step prior to growth. The first technique involved placing the wafer in $(NH_4)_2S$ for 10 minutes in order to passivate the surface and avoid the formation of the native oxide before loading the wafer into the load lock chamber. The other method was to thoroughly rinse the GaAs substrate in deionized water after the H_2SO_4, followed by drying the substrate with N_2. Any native oxide that formed was removed by a pretreatment step in the reactor performed immediately before the growth. Two different pretreatment techniques were explored. The first consisted of a 10 minute exposure of the GaAs wafer to H_2S at 600 ^oC. The other was exposure of the wafer to TPPSe at 450 ^oC for 10 minutes.

3.5.2 *Effect of Wafer Preparation*

The experiments investigating the effect of the wafer preparation were initially performed in order to establish the best way of preparing the GaAs substrates. The 10K photoluminescence spectra of the ZnSe films grown using the three preparation techniques is shown in Figure 3.4. All of the samples were grown at 400 ^oC, with a delivery rate of 5 μmol/min of both TPPSe and DMZn, at a pressure of 300 Torr utilizing a He carrier gas.

As evidenced by Figure 3.4, the substrate preparation had an effect on the photoluminescence of the films. The ZnSe film grown following the 10 min TPPSe

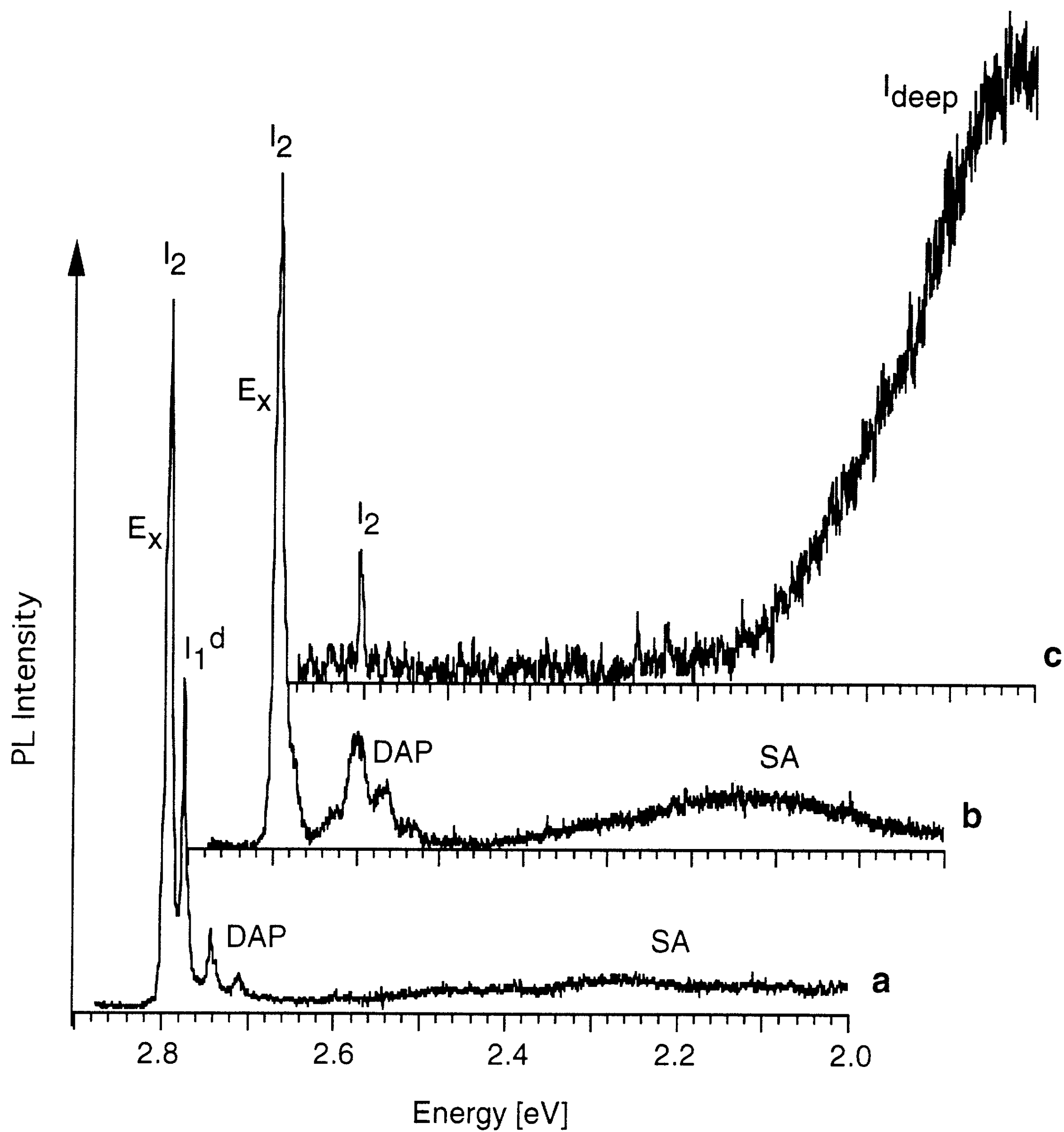

Figure 3.4: 10K PL spectra of ZnSe. The films were grown at 400 ^{o}C with DMZn (5μmol/min) and TPPSe(5μmol/min) in He utilizing three wafer preparation techniques: (a) 10 min TPPSe pretreatment, (b) 10 min H_2S pretreatment, and (c) 10 min $(NH_4)_2S$ passivation.

passivation at 450 °C, exhibits strong near band edge emission, with little deep level emission, a spectra indicative of a high optical quality film. The details on the origin of the various peaks in the near band edge spectra will be discussed in detail in the following sections. The film grown with the 10 min H_2S passivation at 600 °C also demonstrates good photoluminescence, however there is an increased amount of deep level emission (SA), indicative of some degradation in film quality. Furthermore, the donor acceptor pair peaks (DAP) were more pronounced in the H_2S pretreated sample. The film grown using the $(NH_4)_2S$ pretreatment, exhibited the worst PL spectra of the three methods. It is characterized by significant deep level emission, with little near band edge emission, suggesting the poor optical quality of the epitaxially grown film. Based on the superior luminescence of the TPPSe pretreated sample, this preparation technique was utilized for the rest of the growth experiments.

3.5.3 Effect of Growth Temperature

The temperature dependence of the growth rate of the ZnSe films is shown in Figure 3.5. The growth rate is found to range from approximately 0.1 to 1.5 μm/hour in the range of deposition temperatures of 375-500 °C. The growth rate plot demonstrates a change from kinetically controlled growth to mass transport limited growth at approximately 450 °C. The slope of the kinetically controlled portion of the curve indicates an activation energy of approximately 17 kcal/mol.

The growth rates were obtained from a single growth experiment utilizing the in situ laser interferometry technique described in the previous chapter. This allowed for consistent growth conditions, and served to eliminate some of the run to run variability inherent in the OMVPE process. The accuracy and viability of this technique will be addressed in the following chapter. The overall growth rates were relatively slow and found to be limited by the delivery of the TPPSe source. It is believed that a more volatile phosphine selenide source, which would allow higher delivery rates, would increase the growth rate of the ZnSe films.

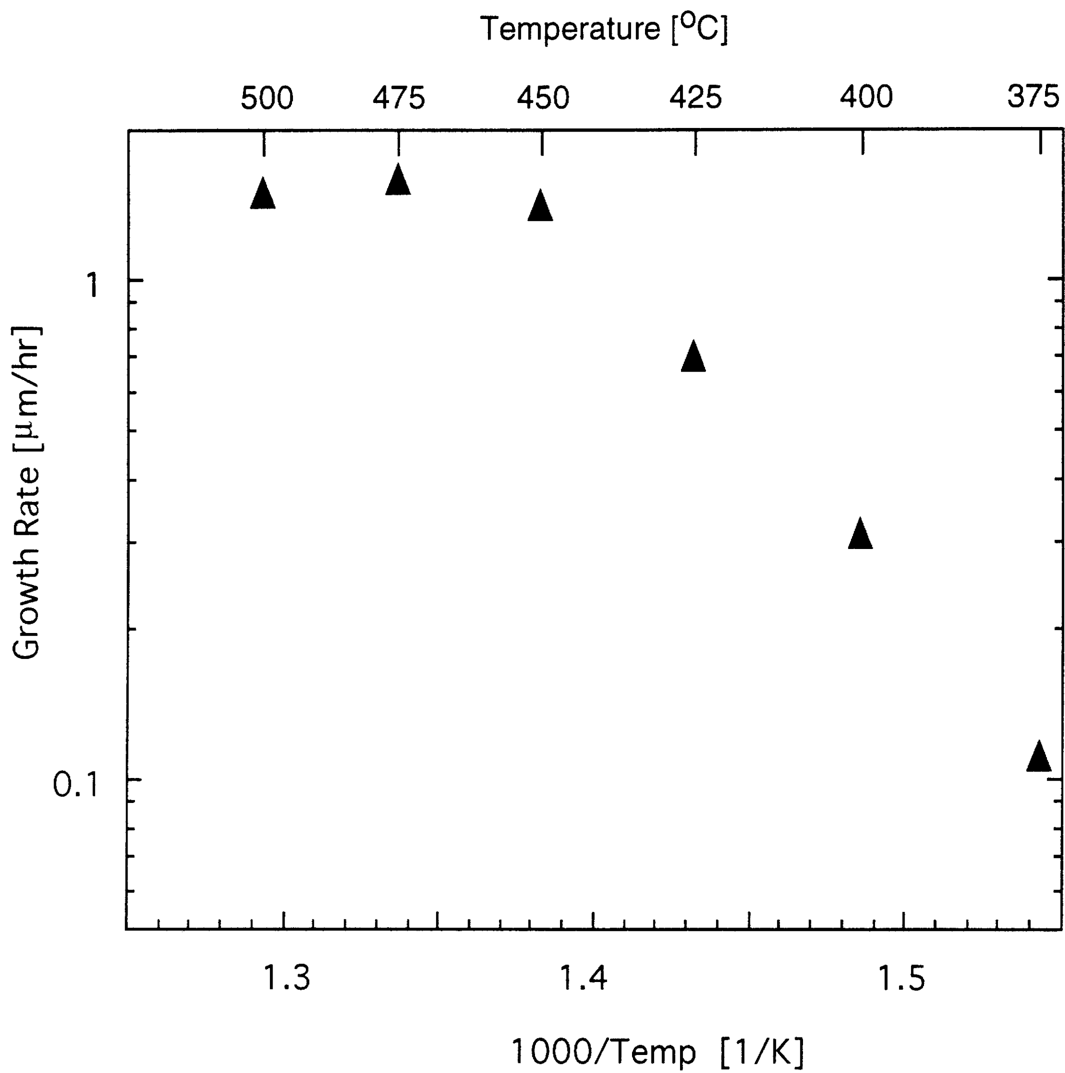

Figure 3.5: Temperature dependence of the ZnSe growth rate in He from DMZn (5 µmol/min) and TPPSe (5 µmol/min).

The effect of the deposition temperature on the surface morphology was investigated by scanning electron microscopy. Figure 3.6 illustrates SEM micrographs of ZnSe films grown at a range of deposition temperatures. All experiments were performed in a He carrier gas at 300 Torr with a delivery rate of 5 μmol/min for both the TPPSe and DMZn sources. All of the samples demonstrate a characteristic "orange peel" morphology. The morphology appears to deteriorate as the growth temperature is increased from 375 °C to 450 °C. It should be noted that the films grown at 375 °C and 400 °C are 0.5 μm thick, while those at 425 °C and 450 °C are 1.0 μm thick. Thus care should be taken comparing the two groups since generally as the epitaxial film becomes thicker its morphology worsens. However, comparing the film grown at 375 °C to the 400 °C sample and the 425 °C sample to the one grown at 450 °C, a general deterioration of the film morphology is observed as the deposition temperature is increased.

Figures 3.7 and 3.8 depict the photoluminescence spectra of the ZnSe films grown at 375-450 °C. The 10K PL of all of the samples in Figure 3.7 are characterized by strong near band edge emission with low amounts of deep level emission. The samples all contain strong donor bound (I_2) excitonic emission lines at 2.796 eV and donor acceptor pair (DAP) peaks at approximately 2.740 eV. While it is difficult to quantitatively compare the absolute emission intensities, there is a decrease in the intensity at 450 °C and this is evidenced by comparison of the peak to noise level. There was also a slight increase in the amount of deep level emission (SA) at 450 °C, indicating a degradation in the optical quality of the epitaxial film as the deposition temperature is increased to 450 °C. The overall low deep level emission in the films is characteristic of high optical quality, with an increase in deep level emission generally indicative of the development of structural defects.

A more detailed look at the near band edge emission of the samples is shown in the 1.9K PL spectra in Figure 3.8. The samples grown at 350 °C and 375 °C are characterized by free excitonic emission (E_x) at 2.801-2.802 eV and a donor bound

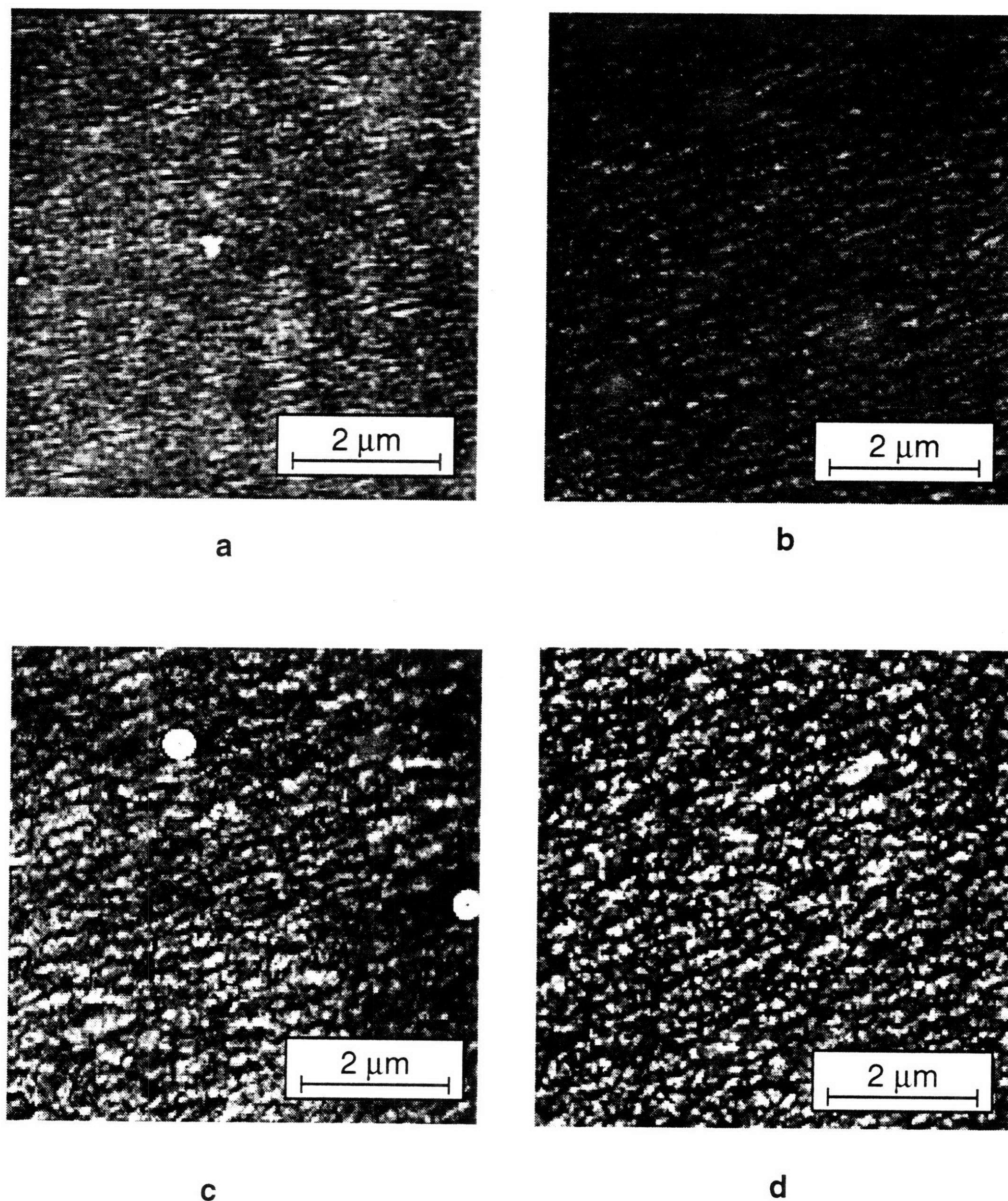

Figure 3.6: SEM micrographs of ZnSe films grown from TPPSe (5µmol/min) and DMZn (5µmol/min) in He at (a) 375 °C, (b) 400 °C, (c) 425 °C, and (d) 450 °C. The layer thicknesses were ~0.5 µm (a,b) and ~1.0 µm (c,d).

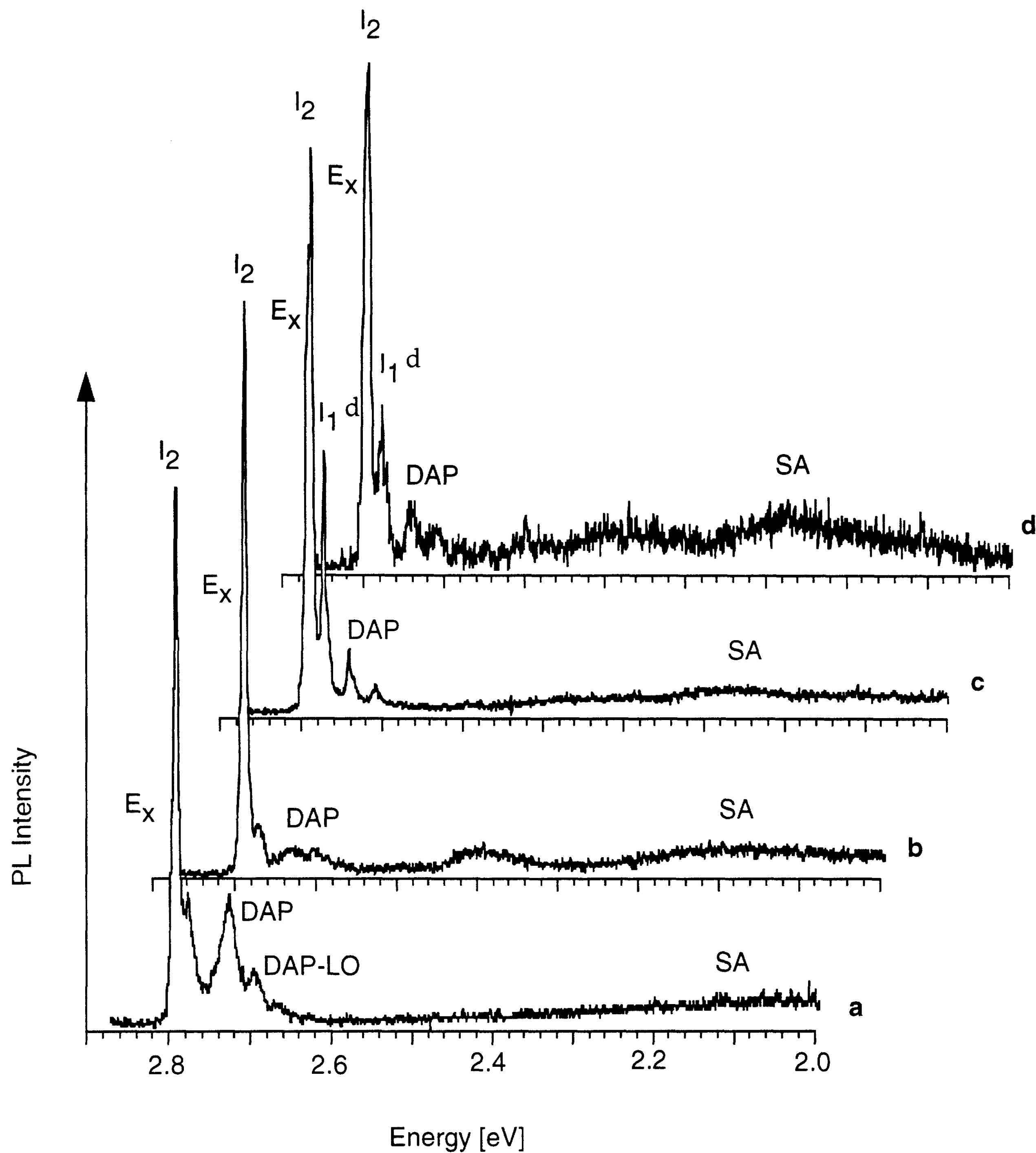

Figure 3.7: 10 K PL spectra of ZnSe. The films were grown from TPPSe (5 μmol/min) and DMZn (5 μmol/min) in He at (a) 375 ^{o}C , (b) 400 ^{o}C, (c) 425 ^{o}C, and (d) 450 ^{o}C.

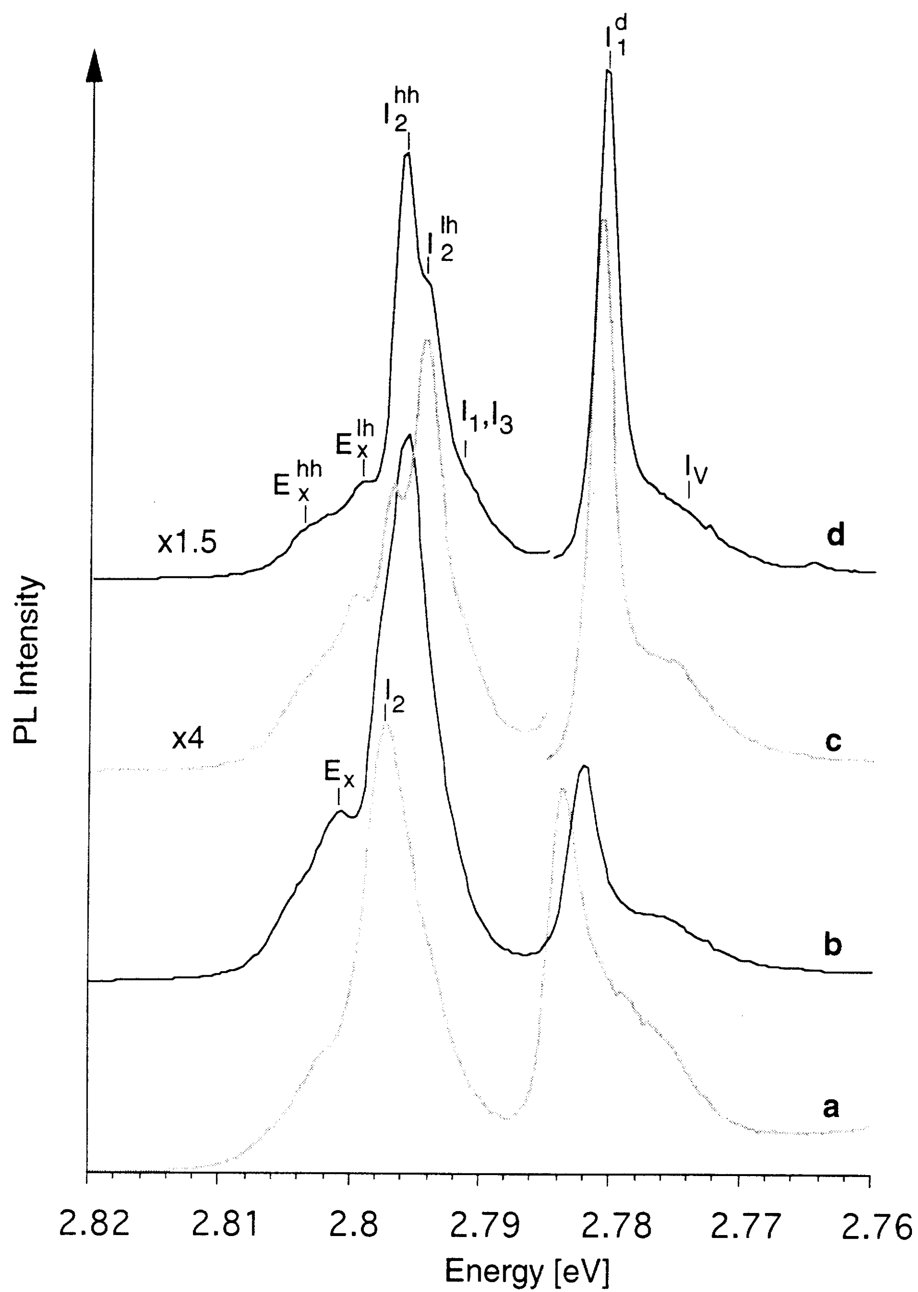

Figure 3.8: 1.9 K near band-edge PL of ZnSe. The films were grown from TPPSe (5 μmol/min) and DMZn (5 μmol/min) in He at various deposition temperatures: (a) 375 °C, (b) 400 °C, (c) 425 °C, and (d) 450 °C.

exciton (I_2) line at 2.796-2.798 eV. While normally there is a splitting of the excitonic lines into heavy holes (hh) and light holes (lh), it is believed that the splitting is not seen in these samples due to the strain from the lattice mismatch compensating the thermal tensile strain. The thermal tensile strain develops from the difference between the thermal expansion coefficients of the ZnSe epitaxial film and the GaAs substrate. [43-45] The lattice mismatch strain originates from the small difference in the lattice constants of ZnSe (5.6684 A) and GaAs (5.6533 A). [46] Normally the lattice mismatch strain relaxes once the epitaxial film is above a critical thickness (h_c), as misfit dislocations form at the interface; however for films below this critical thickness the energy to create these dislocations is greater than the energy required for the film to strain and the epitaxial film will remain in tension or compression. Mitsuishi et al., demonstrated that above a critical thickness of 0.15 μm, the lattice mismatch strain begins to relax, however the epilayer doesn't become fully relaxed until a thickness of approximately 1.0 μm is reached. [47] The films grown at 375 °C and 400 °C were relatively thin (0.5 μm), indicating that the lattice mismatch strain was not fully relaxed, which in turn may have compensated the tensile strain originating from the difference in thermal expansion coefficients. The samples grown at 425 and 450 °C, which were 1.0 μm thick, demonstrate the characteristic free excitonic (E_x^{hh} and E_x^{lh}) and donor bound (I_2^{hh} and I_2^{lh}) excitonic splitting.

The free excitonic emission line located at 2.801 eV is in good agreement with previously published results. [14,48-50] Similarly, the donor bound exciton lines (I_2) are also found to be consistent with previous research.[14,49-51] However, it is difficult to determine the specific origin of the donor bound excitonic emission since many of the ZnSe donor dopant lines fall in similar energy ranges. It is speculated that these lines may originate from Cl or Ga atoms. [52] The Cl atoms could potentially come from the phosphine selenide source. Commercial grade tripropyl phosphine was used for the phosphine selenide synthesis, and chlorinated compounds are typically present in the synthesis of tripropyl phosphine. The Ga impurity atoms may originate from interdiffusion of Ga from the GaAs substrate at the interface. [52]

All of the samples similarly contain I_1^d lines and donor acceptor pair (DAP) peaks. The I_1^d line was located at 2.7805 eV. While the origin of this line has not been universally agreed upon, it has been proposed that it originates from the presence of zinc vacancies(V_{Zn}) associated with neutral donors or copper impurity atom. [53] The presence and origin of this line will be further discussed in the section exploring the effect of the Se/Zn ratio in the gas phase. The DAP emission occurs at approximately 2.734 eV, a position which is consistent with a level attributed to a phosphorous (acceptor) atom bound to a donor atom. [54] This assignment is in line with the potential for phosphorous incorporation from the growth chemistry and will be supported in a subsequent section with secondary ion mass spectroscopy (SIMS) results.

3.5.4 Effect of VI/II Ratio

The effect of changing the Se/Zn ratio, or VI/II ratio, in the gas phase was examined by growth of ZnSe films at 425 °C with ratios of 0.5, 1 and 2. The various ratios were established by utilizing DMZn delivery rates of 2.5, 5, and 10 μmol/min while maintaining the TPPSe delivery rate at 5 μmol/min. The growth rate was found to be insensitive to changes in the DMZn delivery, indicating that growth was limited by the delivery of TPPSe. This was confirmed by a separate growth experiment utilizing the in situ laser interferometry technique. The delivery rate of the TPPSe was incrementally increased and the measured growth rate was found to similarly increase.

The 10K PL spectra and 1.9K near band edge PL spectra are shown in Figures 3.9 and 3.10 respectively. Once again the films are of high optical quality, indicated by the sharp near band edge emission and low amount of deep level emission. The spectra are dominated by strong excitonic emission and small donor acceptor pair (DAP) peaks. The excitonic emission is characterized by free excitonic emission at 2.802 eV and donor bound excitonic emission at 2.796 eV, which is again in good agreement with the samples previously described and the information found in the literature. Similarly, I_1^d lines at 2.780 eV and DAP peaks at approximately 2.740 eV are observed.

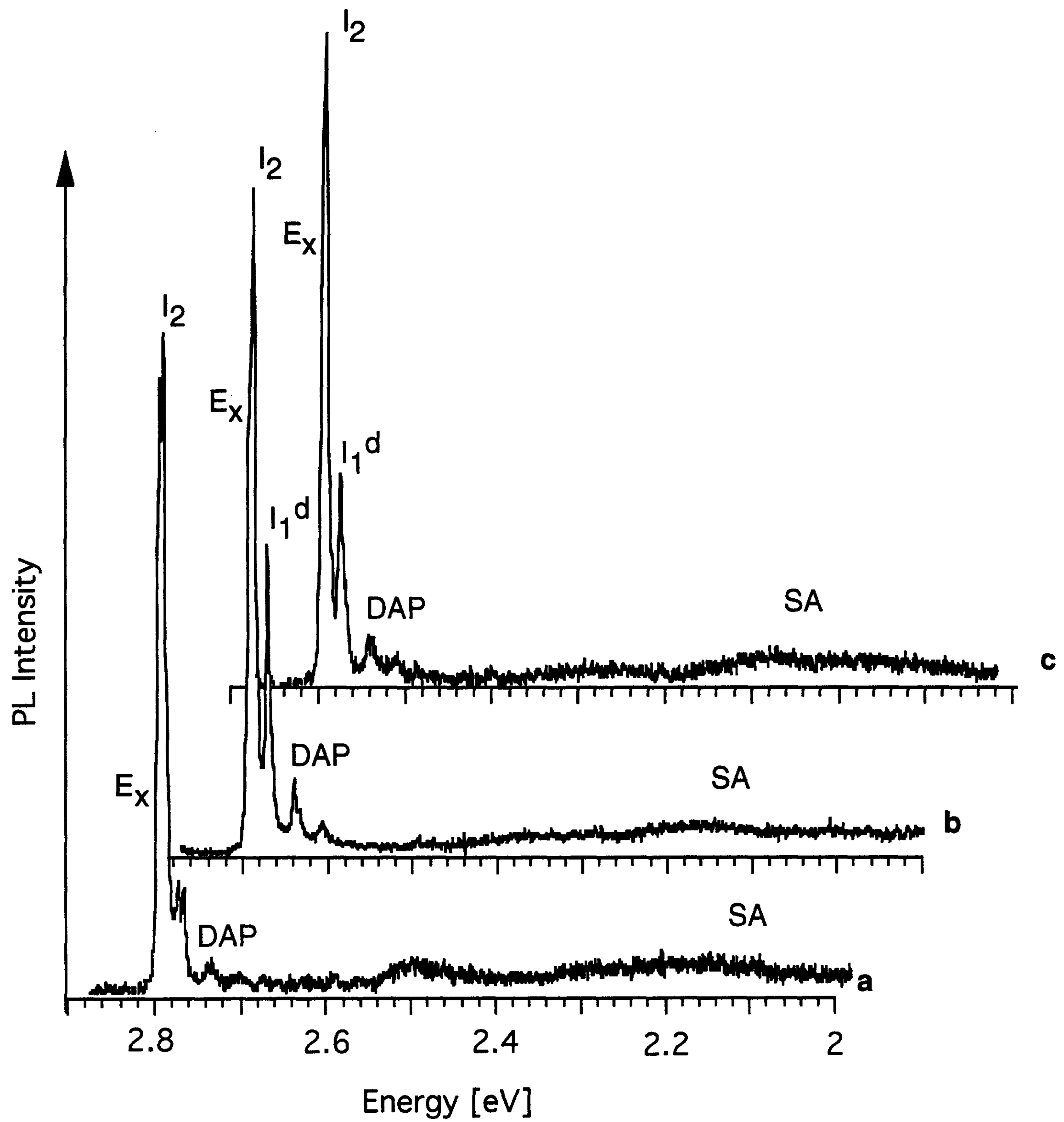

Figure 3.9: 10 K PL spectra of ZnSe. The films were grown at 425 °C from TPPSe (5 μmol/min) and DMZn in He at VI/II ratios of (a) 0.5, (b) 1.0 and (c) 2.0.

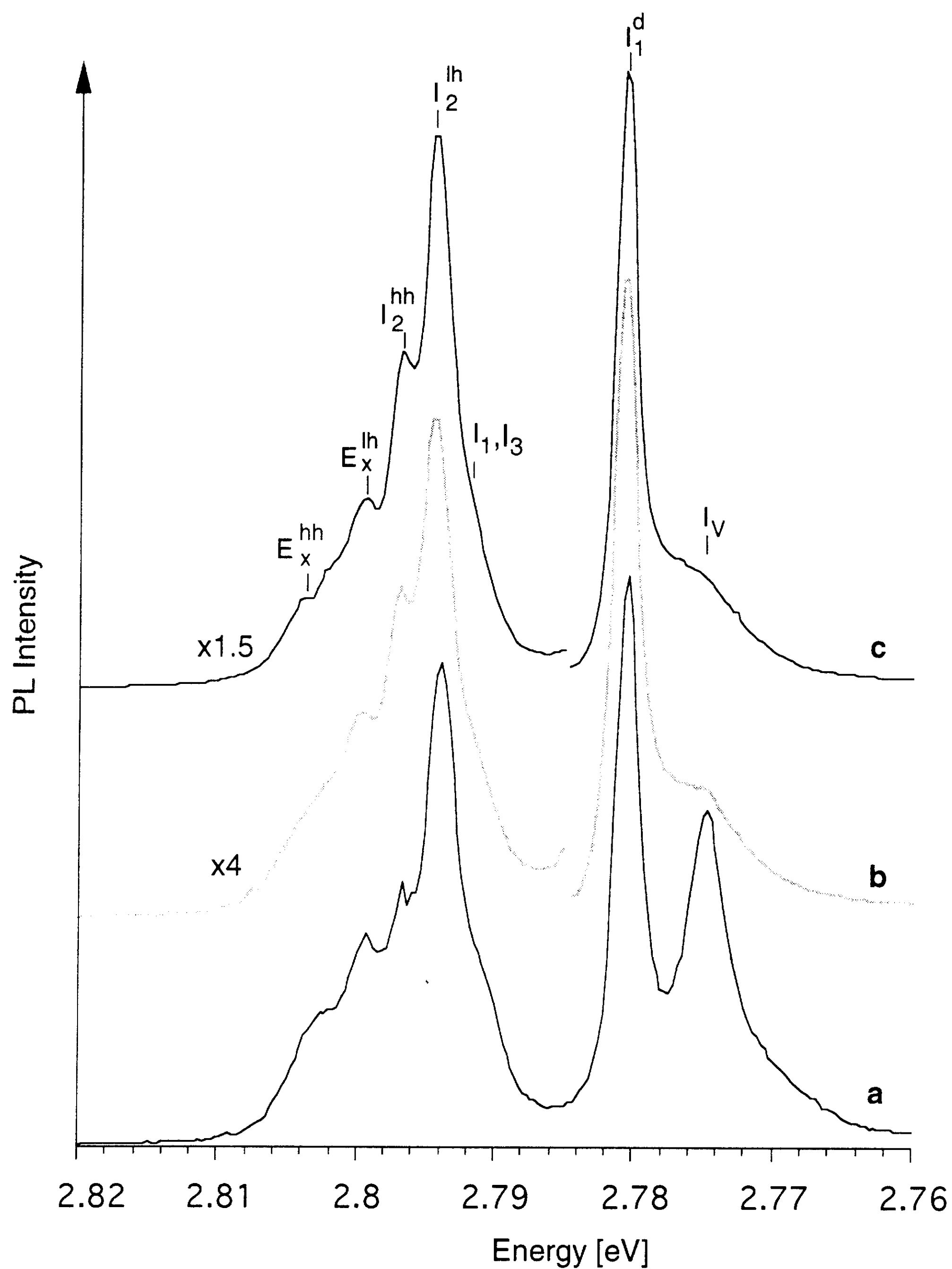

Figure 3.10: 1.9 K near band-edge PL of ZnSe. The films were grown from TPPSe (5 μmol/min) and DMZn in He at 425 °C at VI/II ratios of (a) 0.5, (b) 1.0 and (c) 2.0. The film thicknesses were ~1 μm.

A closer look at the near band edge emission illustrated in Figure 3.10 shows the characteristic splitting of the free and donor bound excitons. This is consistent with the fact that the 1.0 μm thick samples have the lattice mismatch strain relaxed; the splitting is caused by the thermal tensile strain described earlier. The I_1^d line has been proposed to originate from zinc vacancies associated with either neutral donor atoms or Cu atoms. [55] The behavior of the I_1^d lines as the Se/Zn ratio is changed conforms with this explanation. As Zn rich conditions are approached, that is the VI/II ratio is decreased, there is a reduction in intensity of the I_1^d line. The shoulder of the I_2 peak can be attributed to either shallow acceptor bound excitons (I_1), which is consistent with low levels of phosphorous incorporation [22], or excitons bound to ionized donors (I_3) [54]. Finally, the shoulder of this peak, labeled I_v is believed to be attributed to selenium anti-site defects. [56]

3.5.5 H, C and P Incorporation

Secondary ion mass spectroscopy (SIMS) was performed to determine the incorporation of impurity atoms in the ZnSe epitaxial films. The results are illustrated in Figure 3.11. A ZnSe film grown from TPPSe at 400 °C and DMZn was compared to the incorporation levels of a ZnSe film grown from tBASe and DMZn:NEt_3, a precursor chemistry previously investigated to reduce the level of carbon incorporation. [57]

The hydrogen, carbon, and phosphorous incorporation profiles of the TPPSe sample exhibit a common trend. There is a high level of the impurity atoms at the surface, followed by a drop off in the bulk and then an increase at the ZnSe/GaAs interface. These results are consistent with the growth procedure. The GaAs substrates were pretreated with a 10 minute exposure to TPPSe at 450 °C and this is likely the origin of the higher incorporation levels at the interface. An alternative explanation, may be the presence of defects at the ZnSe/GaAs interface arising from the slight lattice mismatch. It has been previously reported that increased impurity levels have been found at this interface for other growth chemistries. [58] Growth was terminated by

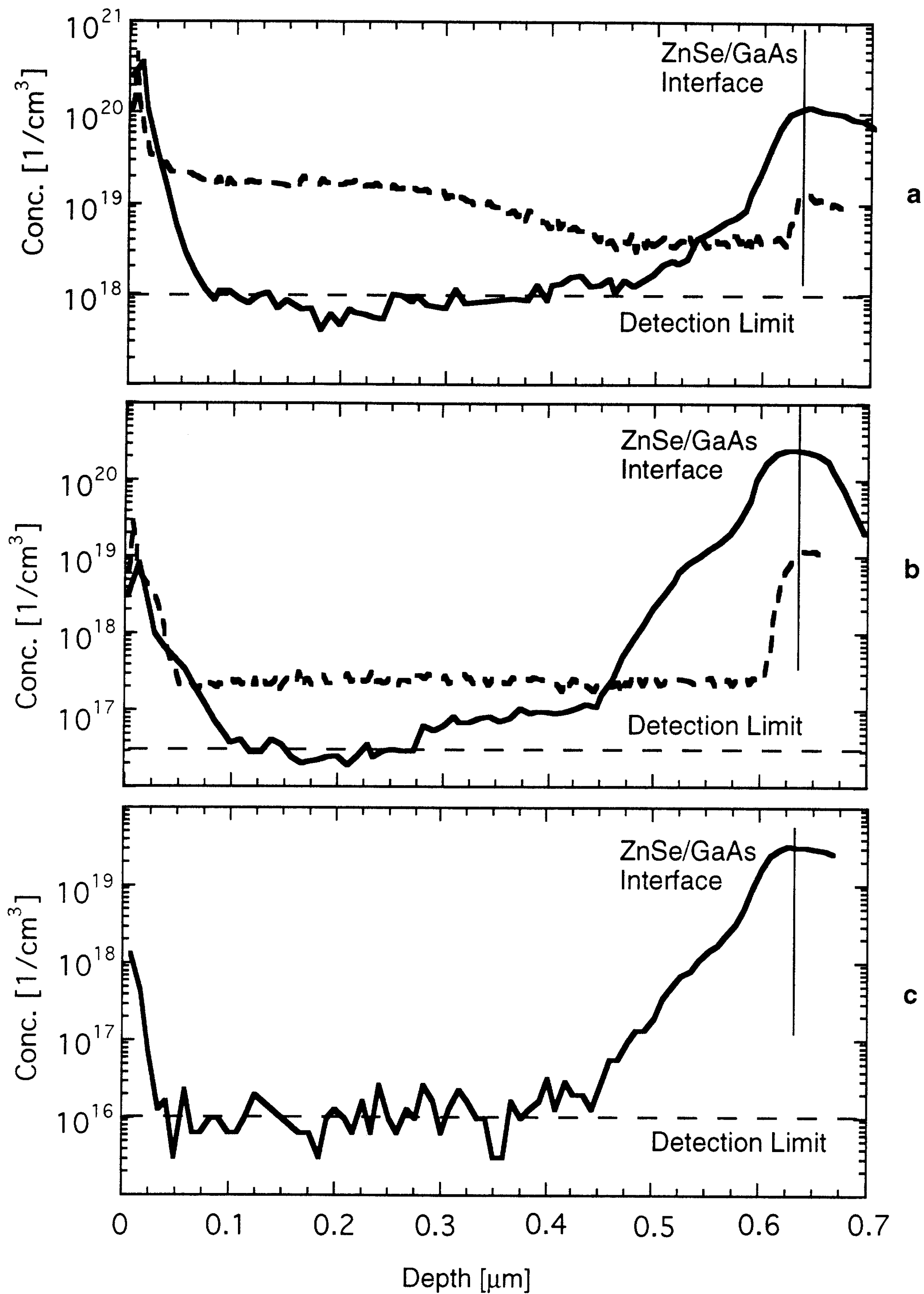

Figure 3.11: SIMS concentration profiles for (a) hydrogen, (b) carbon, and (c) phosphorous for a ZnSe film grown in He with DMZn (5 μmol/min) and TPPSe (5 μmol/min) at 400 °C (———), and a film grown in H_2 from tBASe(40 μmol/min) and DMZn:NEt_3 (20 μmol/min) at 350 °C (— — —).

diverting the DMZn vapor to an exhaust line while the TPPSe vapor continued to flow over the wafer until the temperature was ramped down. It seems likely that the presence of the phosphine selenide during the cool down was the origin of the increased incorporation levels at the surface as well.

The overall concentration of carbon in the bulk of the TPPSe film was found to be approximately 2×10^{16} /cm^3, which is at the detection limit of the measurement. This is a low level of carbon incorporation, an order of magnitude lower than carbon level of 2×10^{17} /cm^3 in the film grown from tBASe, a precursor utilized to lower carbon incorporation. While impurity carbon atoms in ZnSe are neither active electrically or optically [59], it is important to limit the amount of carbon incorporation in the films to insure the high structural quality of the films which will be important in the overall performance of ZnSe devices.

The phosphorous incorporation level in the bulk was observed at the detection limit of 10^{16} /cm^3 of the SIMS measurement. It is critical to limit the incorporation of phosphorous in ZnSe. While phosphorous is found to be a shallow acceptor at low concentrations (below 10^{16} /cm^3), at higher concentrations it becomes a deep level acceptor. [48] The presence of the DAP peaks in the PL spectra, previously associated with shallow phosphorous acceptor atoms bound to a donor impurity atom, combined with the low levels of incorporation observed with the SIMS measurements, suggest that any phosphorous atoms that are incorporating in the ZnSe are in the shallow acceptor level. The carbon and phosphorous profiles lend further credence to the proposed growth chemistry; the lack of P and C atoms in the bulk of the film indicates that the phosphine is not significantly donating P and C impurity atoms and is likely a stable byproduct of the growth process.

Finally, the TPPSe sample at 400 ^{o}C exhibits a low level of H incorporation. The level of 1×10^{18} /cm^3 in the bulk is once again at the detection limit of the measurement and is the lowest concentration known to the author to be published. The level is nearly an order of magnitude lower than the level of approximately 1×10^{19} /cm^3 observed in

the sample grown from the tBASe source. Hydrogen incorporation levels of 10^{19} - $10^{20}/cm^3$ have been reported for ZnSe growth using methylallylselenide (MASe). [54] Since it was the objective of these growth experiments to demonstrate the potential for these phosphine precursors to be utilized for hydrogen free p-type ZnSe, the SIMS results, in conjunction with the PL measurements, indicate that a significant first step has been made.

3.5.6 Effect of Carrier Gas

Ultra high purity helium was chosen as the carrier gas since He is inert and therefore would not interact with the growth process. H_2 carrier gas is commonly used in OMVPE growth, and while H_2 alone is thermally stable at the deposition temperatures of these experiments, it was investigated to determine if there were any carrier gas interactions with the growth chemistry. ZnSe growth was performed at 425 ^oC with a delivery rate of 5 μmol/min of both the TPPSe and DMZn sources. The growth rate of the ZnSe film was found to dramatically increase in the presence of the H_2 carrier gas. The growth rate was 5 μm/hr, compared to 0.8 μm/hr with the He carrier gas. There was also significant wall deposit during the growth in H_2, something not observed in He until a deposition temperature of 475 ^oC was reached.

The 10K PL spectra of films grown in H_2 and He carrier gases are shown in Figure 3.12. A dramatic change in both the near band edge emission and deep level emission is evident. The sample grown in H_2 exhibits a dramatic increase in DAP emission. The deep level (I_{deep}) band centered at 2.0 eV is consistent with P in its deep acceptor state. [22,60] SIMS analysis of this film, along with a sample grown in He at 400 ^oC can be seen in Fig 3.13. While the deposition temperatures are not the same and caution should be taken in comparing the two results, there are dramatic increases in the hydrogen and phosphorous incorporation levels. There was a marked change in the incorporation of phosphorous atoms in the film, increasing from the detection limit of $10^{16}/cm^3$ in He to a level of approximately $4 \times 10^{18}/cm^3$ in H_2. The hydrogen

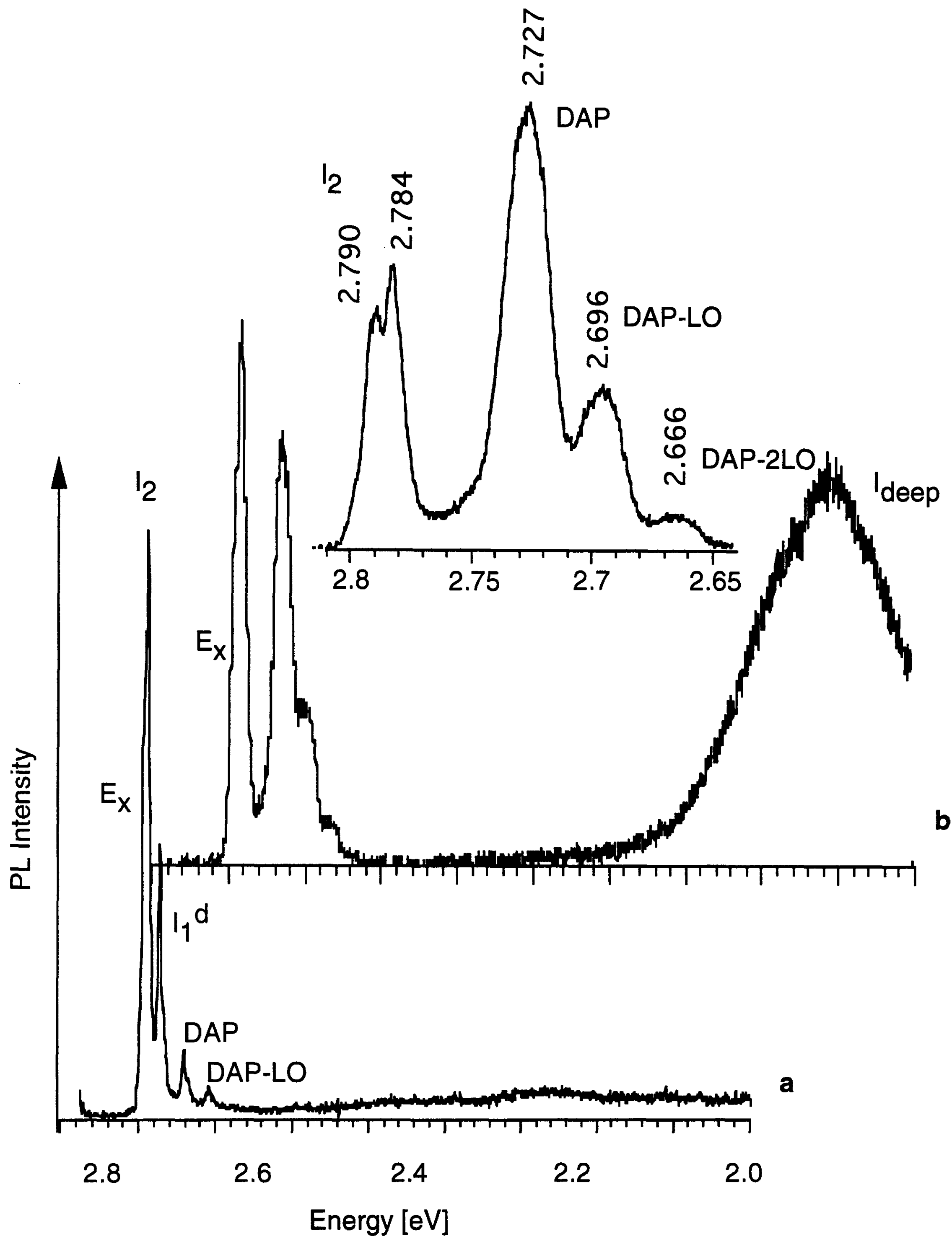

Figure 3.12: 10K PL spectra of ZnSe. The films were grown at 425 °C from DMZn (5 µmol/min) and TPPSe (5 µmol/min) in (a) He and (b) H_2. Also shown is a more detailed spectra of the near band edge of the sample grown in H_2.

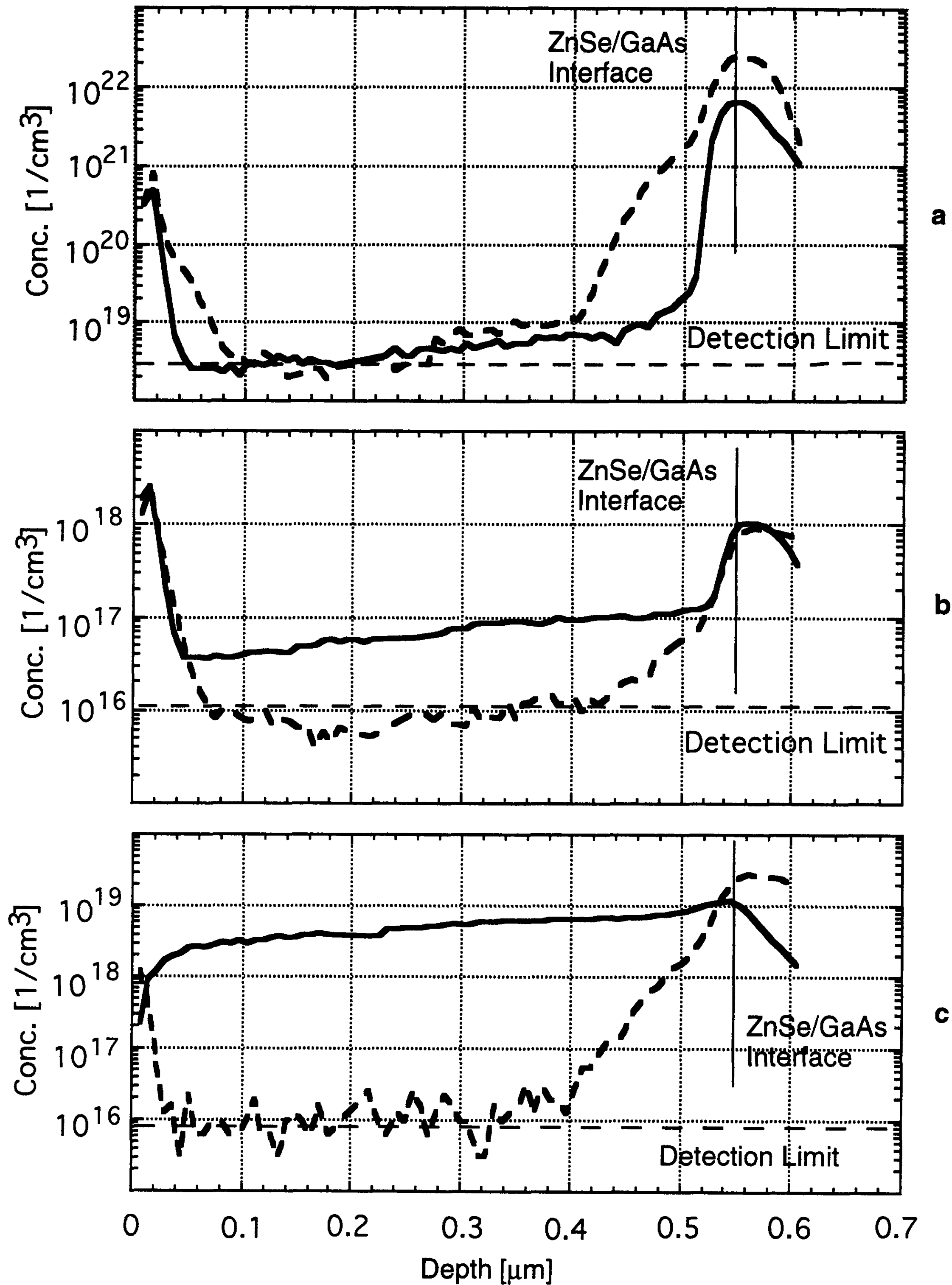

Figure 3.13: SIMS concentration profiles for (a) hydrogen, (b) carbon and (c) phosphorous for ZnSe films grown from TPPSe (5 µmol/min) and DMZn (5 µmol/min) at 425 °C in He (— — —),and H_2 (———).

incorporation, which was at the detection limit in the sample grown in He, was found to increase to a level of $5 \times 10^{18}/cm^3$ in the ZnSe film grown in H_2. Strangely, the incorporation level of carbon was not observed to increase, remaining at a level near the detection limit of the measurement. The lack of an increased level of carbon incorporation may be related to a free radical chemistry, where the phosphine molecule is attacked by a hydrogen radical, leading to an increased level of phosphorous, while the remaining organic group goes to the exhaust.

The combination of SIMS, PL and growth rate results all lead to the conclusion that the growth chemistry has been altered in the presence of a hydrogen carrier gas. Furthermore, the dramatic increases in P and H would appear to indicate that the tripropyl phosphine is no longer a stable byproduct of this reaction. It should be noted that changing the carrier gas has been found to have an effect on the growth chemistry of ZnSe utilizing other precursors. Kuhn et al, detail a change in the incorporation levels of carbon and hydrogen in films grown from MASe and DEZn when the carrier gas was changed from H_2 to He. [14] Both the H and C incorporation levels were found to change by an order of magnitude. However, for the MASe and DEZn system, the levels were found to decrease in the presence of H_2.

3.6 Growth Results with DMBPSe

While the vapor pressure of dimethyl(butyl)phosphine selenide (DMBPSe), is still too low to be a practical source for the OMVPE growth of ZnSe, it was explored to further test the trialkyl phosphine selenide approach. Furthermore, it demonstrates the potential to find higher volatility compounds by exploring alternative asymmetric phosphines.

Due to the limited amount of the source material, only a few experiments were able to be performed. The growth rate of ZnSe from DMBPSe and DMZn in He was found to be consistent with that of the TPPSe source. Similarly, the surface morphology

of a sample grown at 425 °C had the characteristic "orange peel" texture and was comparable to that grown from the TPPSe source at 425 °C. The growth rate results and SEM micrographs comparing the surface morphologies are summarized in Figure 3.14.

The 10 K photoluminescence spectra of samples grown from DMBPSe and TPPSe are shown in Figure3.15. The DMBPSe spectra is quite similar to the TPPSe film and is indicative of a high optical quality epitaxial film. The near band edge emission is consistent with the previous results; free excitonic emission is observed at 2.802 eV, a donor bound exciton (I_2) peak at 2.798 eV and an I_1^d line at 2.781 eV followed by a DAP peak and its phonon replica (DAP-LO). While the donor bound excitonic line was attributed to potential Cl impurities originating from the TPPSe compound, similar Cl contamination problems may exist with the synthesis of the DMBPSe source.

The SIMS profiles for the hydrogen, carbon and phosphorous incorporation levels of a DMBPSe sample are summarized and compared to a TPPSe sample in Figure 3.16. It should be noted that the growth temperature of the DMBPSe sample was 425 °C, while the TPPSe was grown at 400 °C. Once again, the results between the two films are quite similar. The DMBPSe profiles show high incorporation levels at the surface and at the ZnSe/GaAs interface, which is consistent with the 10 min DMBPSe pretreatment step at 450 °C prior to growth and the presence of DMBPSe during the cool down after growth. There was a slight increase in the concentration of phosphorous in the bulk of the film in the DMBPSe sample, $3 \times 10^{17}/cm^3$, however it remains very close to the detection limit and it was already pointed out that the two samples were not grown at the same temperature. The level of carbon was found to remain at the detection limit of the measurement, approximately $6 \times 10^{16}/cm^3$ and likewise the hydrogen level was found to remain at the detection limit, $10^{18}/cm^3$.

The similarities in the SIMS, PL and growth rate results are strong indications that the use of DMBPSe as an alternative phosphine selenide precursor did not significantly affect the growth chemistry and demonstrates the potential of finding and utilizing more volatile trialkyl phosphine selenide precursors.

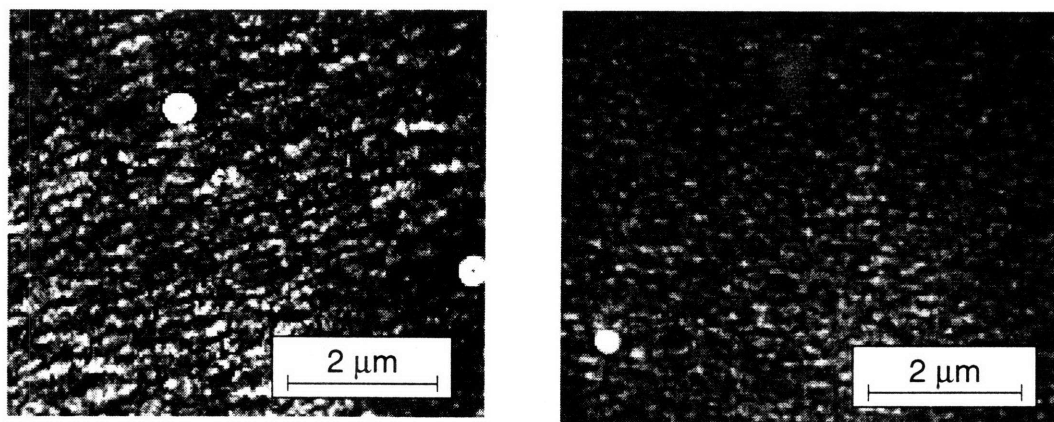

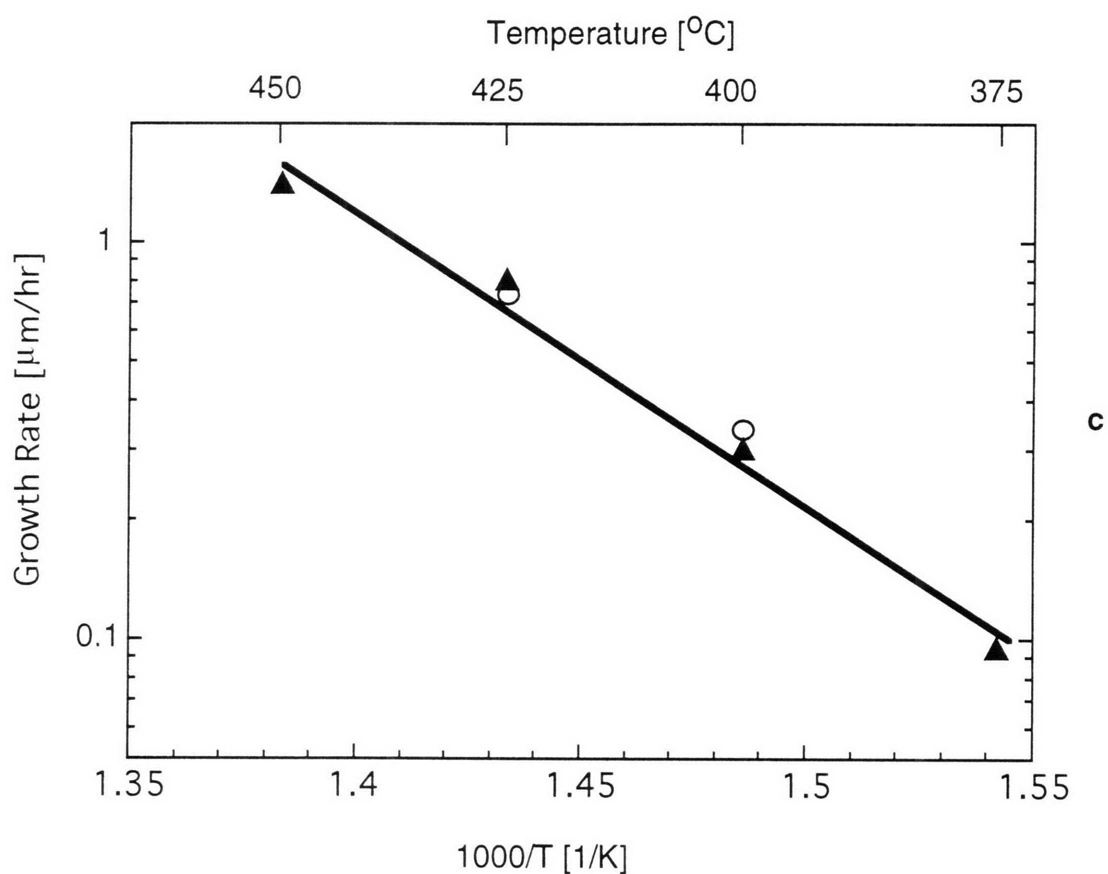

Figure 3.14: SEM micrographs of ZnSe films grown at 425 °C in He from DMZn (5 μmol/min) and (a)TPPSe and (b)DMBPSe, each 5 μmol/min; (c) Comparison of growth rates of ZnSe films grown in He from DMZn (5 μmol/min) and TPPSe (▲) and DMBPSe (O), each 5 μmol/min.

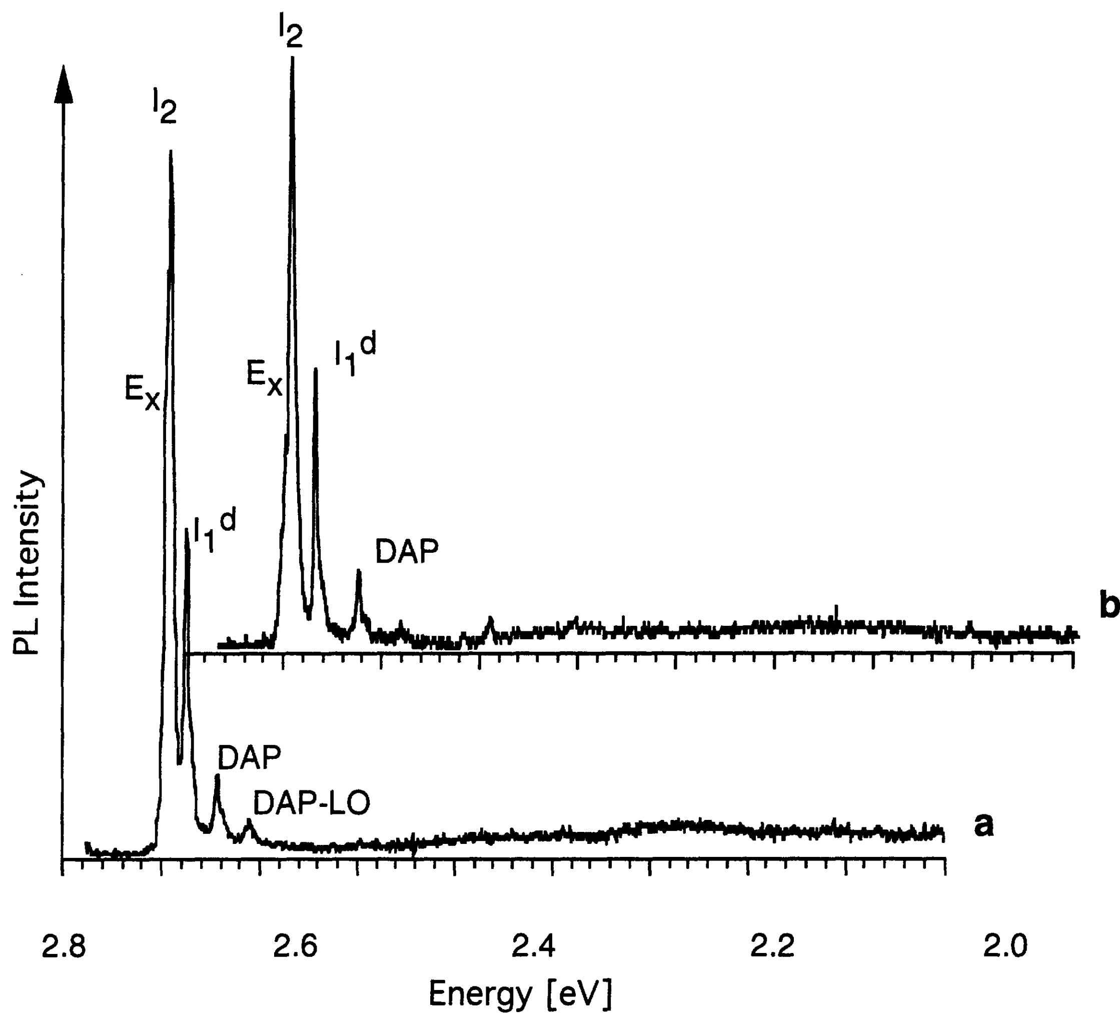

Figure 3.15: 10K PL spectra of ZnSe. The films were grown at 425 °C in He from DMZn (5 µmol/min) with (a) TPPSe and (b) DMBPSe, each 5 µmol/min.

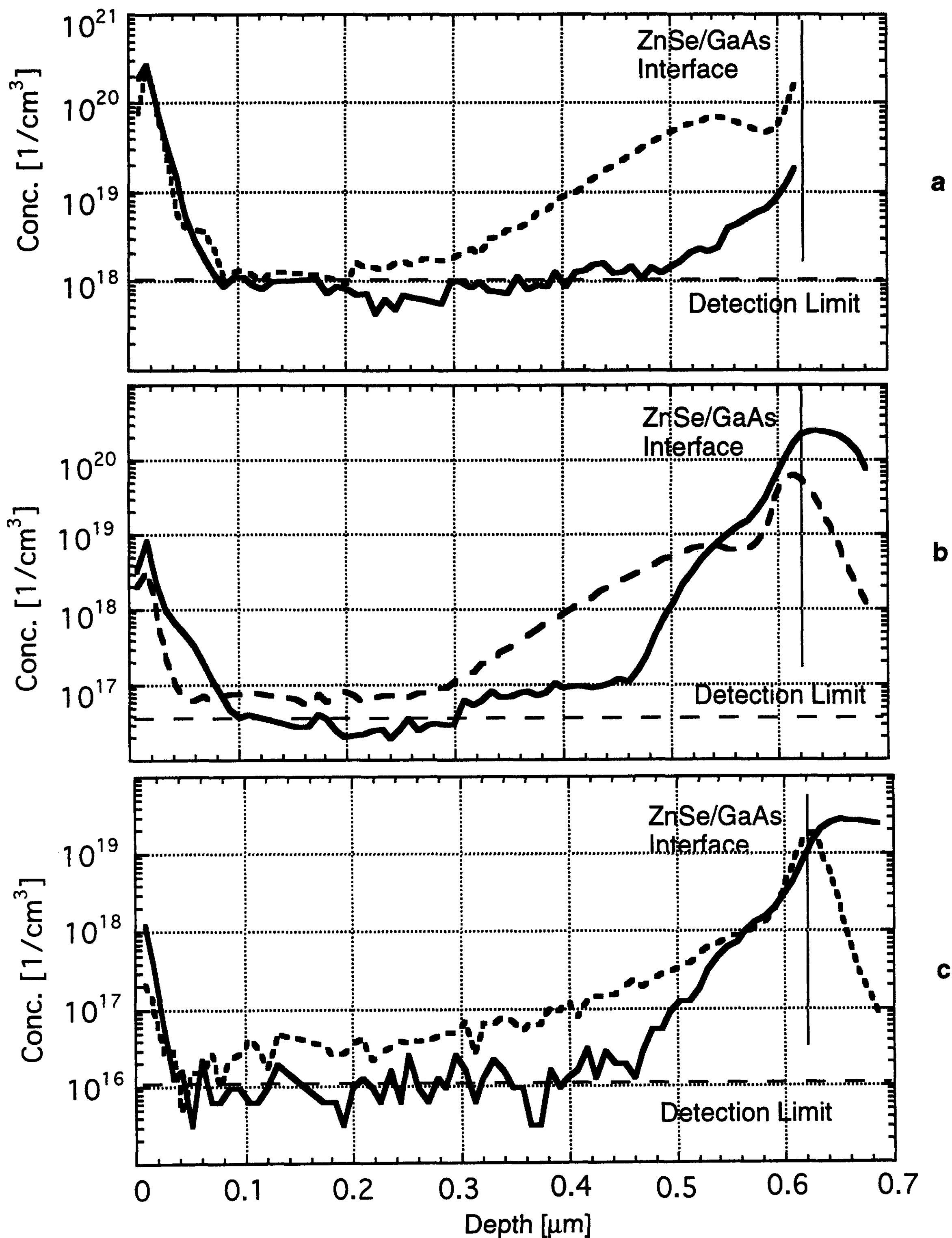

Figure 3.16: SIMS concentration profiles for (a) hydrogen, (b) carbon, and (c) phosphorous for ZnSe films grown in He with DMZn (5 µmol/min) and TPPSe (———) at 400 °C and DMBPSe (— —) at 425 °C, each 5 µmol/min.

3.7 Initial Studies of TMSAZ Doping Source

Initial studies of TMSAZ as a potential nitrogen doping source was investigated. Several problems were encountered with the use of this source. Due to the vapor pressure of the source and the mass flow controllers available, the delivery rate of this precursor was ~5×10^{-3} μmol/min. While one part per thousand is a high ratio for doping, it was consistent with an earlier investigation of this source with H_2Se and DMZn. [42]

Growth of ZnSe from TPPSe, DMZn and the TMSAZ source in a He carrier gas at 400 °C yielded nearly a 10 fold increase in the growth rate, ~6 μm/hr. Furthermore, there was significant wall deposit during the growth, quite similar to that observed of the earlier growth results utilizing the H_2 carrier gas. The photoluminescence spectra of a sample grown utilizing the TMSAZ doping source is compared to a similar film without the source in Figure 3.17. The photoluminescence exhibits markedly increased amounts of deep level emission, indicating a serious degradation of film quality. There is a reduced amount of near band edge emission, with a donor bound excitonic peak located at 2.798 eV. A broad band centered at approximately 2.70 eV can also be observed which is tentatively attributed to donor acceptor pairs. The Y_0 peak, located at 2.60 eV, has been associated with dislocations in the film. [61] While the TMSAZ source constituted only one part per thousand in the gas phase, based on the PL and growth rate results, there was a dramatic change in the growth chemistry. Further studies, investigating the effect of the concentration of TMSAZ in the gas phase, are necessary.

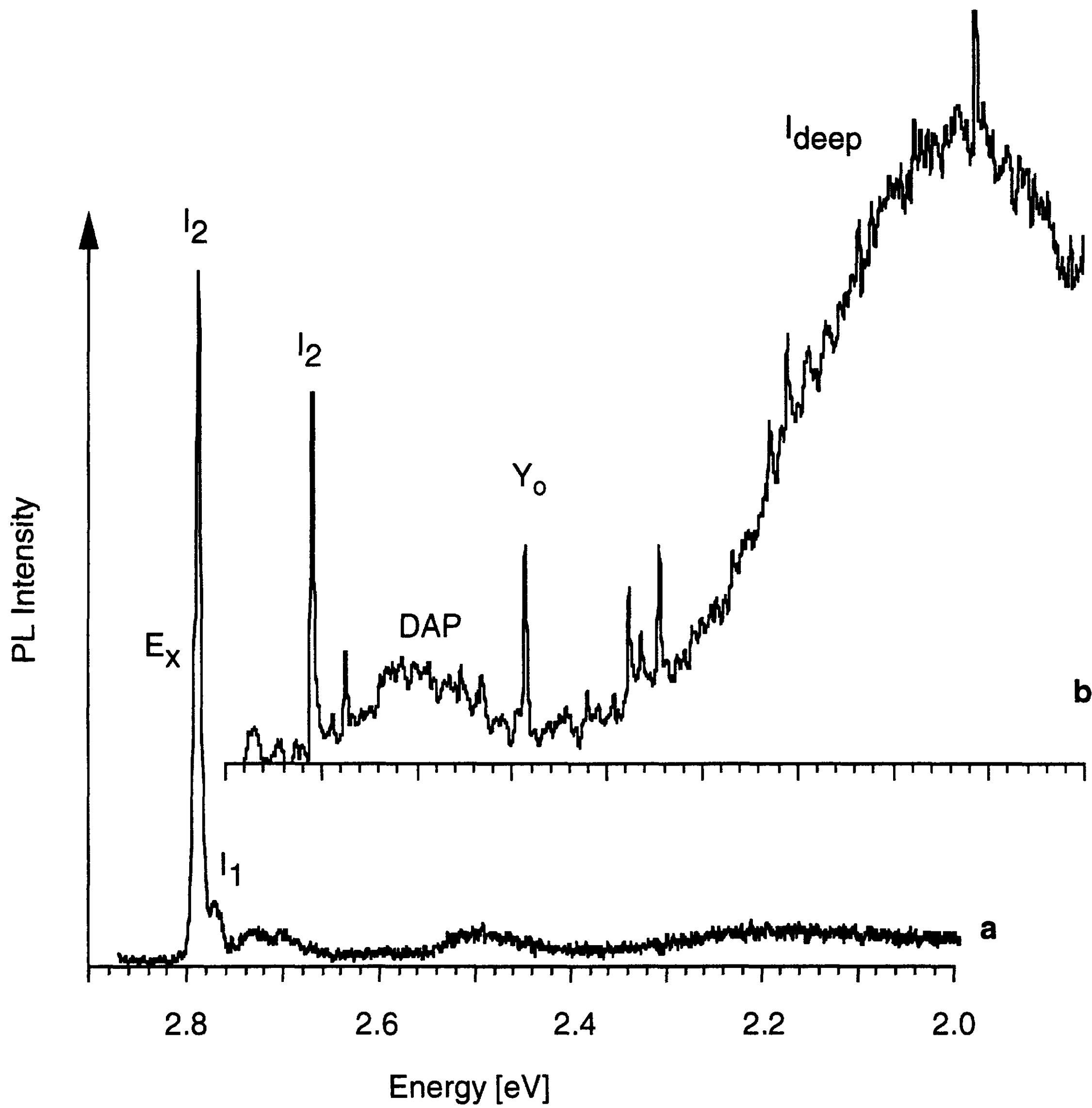

Figure 3.17: 10K PL spectraof ZnSe. The films were grown at 400 °C in He from DMZn (5 μmol/min) and TPPSe (5 μmol/min); (a) undoped and (b) TMSAZ doped (5 x 10^{-3} μmol/min).

4 Optical Monitoring Techniques

4.1 ZnSe Laser Interferometry

4.1.1 Experimental Setup

A schematic of the in situ ZnSe interferometry setup can be seen in Figure 4.1. It is comprised of a 2 mW He-Ne laser, a beam splitter and a silicon photodetector whose output was measured with a chart recorder. The 632.8 nm laser beam was directed into the reactor through a 1/4 inch diameter optical window, was reflected by the wafer back through the window and beam splitter, and then collected by the silicon photodetector. While the use of the beam splitter resulted in a reduction of light intensity of a factor of four, it was necessary due to the geometry of the system. The laser light can be incident on the sample at any angle, however the optical window on this particular reactor was located directly above the sample, which required the light to be normal to the substrate. Care was taken to avoid collection of a reflected beam off of the optical window. The output of the chart recorder was a plot of the reflected beam intensity as a function of time, which allowed the in situ monitoring of the growth rate. Typical light intensities ranged from 20-60 mVolts.

4.1.2 Interferometry Results

Growth Rate Measurements

The accuracy of the in situ laser interferometry technique was checked by SEM analysis of the film thicknesses. A typical chart recorder output of the in situ measurement, as well as an SEM micrograph of a cleaved edge of the same sample is shown in Figure 4.2. The film thicknesses of the in situ measurement and the SEM measurement for several ZnSe samples are summarized in Figure 4.3. As can be seen by a comparison of the two sets of results, the in situ laser interferometry is in good agreement with the SEM analysis.

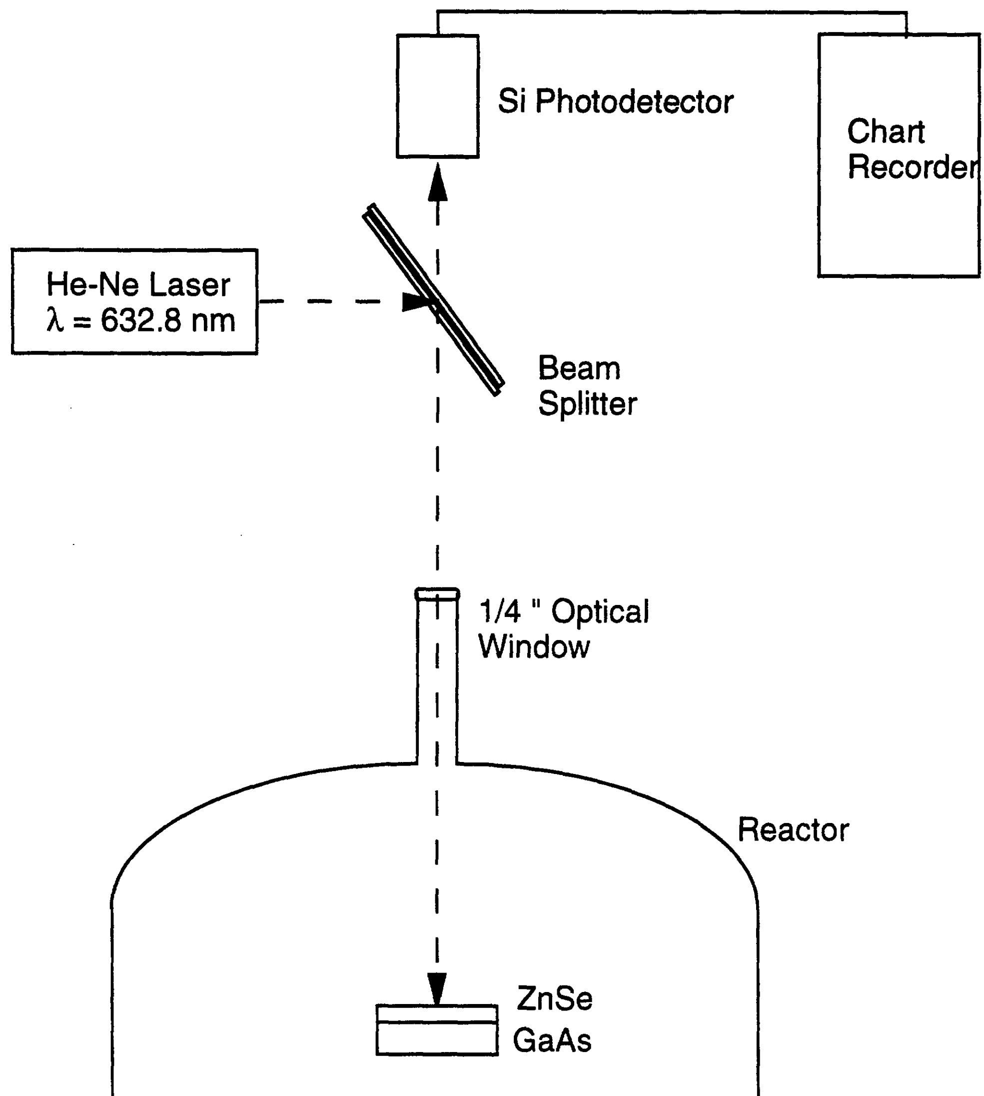

Figure 4.1: Schematic of in situ laser interferometery setup.

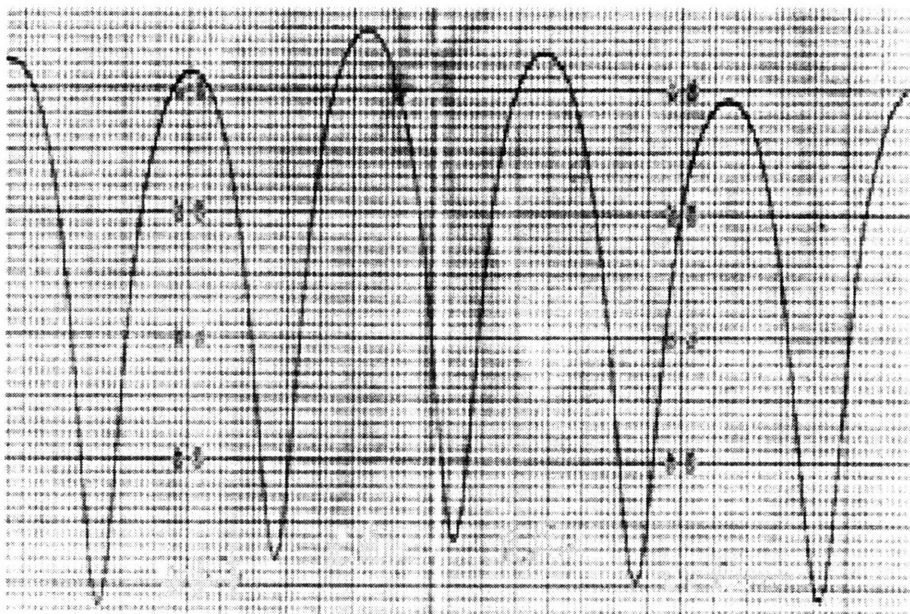

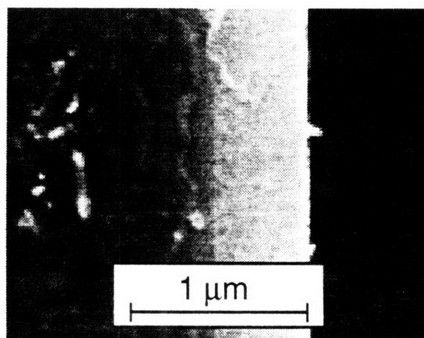

Figure 4.2: Typical laser interferometry output and an SEM image of the cleaved edge of a ZnSe film grown on a GaAs substrate. The interferometry output is a measure of light intensity (mV) as a function of time. Each period represents 0.109 μm growth of the epilayer.

Sample	In Situ Measure. (μm)	SEM Measure. (μm)	Difference (%)
2/22/94	1.108	1.112	1.8
3/13/94	1.105	1.126	0.3
7/11/94	0.981	0.962	1.9
8/2/94	0.545	0.530	2.8
8/26/94	0.545	0.550	0.9

Figure 4.3: Comparison of in situ laser interferometry thickness measurement with SEM measurement of the thickness of the epilayer of a cleaved sample for various ZnSe films.

There are several potential sources for discrepancy between the two results which should be considered if this measurement is to be used for precise control of layer thicknesses. The first consideration is the choice of the index of refraction of the epilayer, n_1. For the calculations performed in this thesis, the room temperature value for the ZnSe index of refraction was used. However, the measurement is performed at the deposition temperature, not room temperature. Since the index of refraction of a material is a function of temperature, the value at the deposition temperature should be used. For ZnSe, the temperature dependence of the index of refraction of ZnSe is quite insensitive. For this reason along with the fact that very precise thickness measurements were not required, the room temperature value was utilized for convenience. Another potential problem in the investigation of other material systems is that information on the temperature dependence of the index of refraction is not always available and several experiments at each deposition temperature, along with measurements of the film thickness, would be needed to determine this value.

Another source of discrepancy is the positioning of the sample and the incident laser beam. For this particular reactor, the 1/4" optical window limited the ability to position the laser beam on the sample. Since the sample was transferred from the load lock chamber to the growth chamber by a magnetically coupled arm, there was the possibility of slight movements of the 1 cm^2 sample on the susceptor. Thus the in situ measurement was not always made in the same position on the sample. Measurements that may be made close to the edge of a sample could potentially lead to slight changes in the thickness measurements. For the SEM analysis, the samples were cleaved in half, and thus film thickness at the center of the sample were measured. If more precise measurements are required it is necessary to keep the position of the laser beam on the sample more consistent. This could be accomplished either by careful positioning of the substrate on the susceptor or the use of a larger optical window which would allow more latitude in the positioning of the laser beam.

One of the significant advantages of this technique for the work done in this thesis was the ability to perform measurements of several growth conditions during a single growth experiment. This is particularly useful for investigation of new sources, where there typically is a limited amount of the source available.

Furthermore, a rough window of operating conditions can be determined with just a few growth experiments, saving both research time and resources.

An example of this was the determination of appropriate deposition temperatures for the new phosphine selenide precursors. While knowledge of the bond strengths in the molecule may provide an educated guess of an appropriate growth temperature, there is still a large degree of uncertainty. The measurement of the effect of temperature on the growth rate of ZnSe presented in Figure 3.5 in the previous chapter was obtained from a single growth experiment. The temperature was stepped up in intervals of 25 ^oC while the growth rate was monitored in situ. In this manner, appropriate deposition temperatures, as well as the delivery rates of the precursors can be investigated in just a few experiments rather than performing a single experiment for each deposition temperature and each change in the delivery rate.

Is the measurement of several growth rates in a single experiment valid? In Figure 4.4 the temperature dependence of the growth rate of ZnSe is replotted along with the growth rates measured during individual runs. As evidenced by the figure, the results are in good agreement. The use of the in situ measurement to investigate several variables in a single growth experiment should be performed with caution however. Several potential problems with the measurement of the growth rate can arise. One factor that must be considered is the initial nucleation of the epitaxial film. In nearly all of the experiments, the time of the first interference period was slightly longer than subsequent ones. This may potentially skew the growth rate measurement of the first variable investigated. In order to avoid this potential source of error when investigating the effect of growth temperature, approximately 0.2 μm of ZnSe film was grown at the first temperature before making the in situ measurement. Additionally, two to three interference cycles were averaged at each temperature in determining the growth rate. A second problem may arise from a deterioration of the surface morphology of the film. As the epitaxial film grows, the film surface tends to roughen, which may lead to increased growth rates. The identification of this problem is more difficult, however, as will be seen in the next section, the intensity output of the light yields some information in regards to this problem. Based on the agreement between the overall experiment with the individual experiments. surface roughening was not a significant problem. For the purposes of establishing an operating window, the in

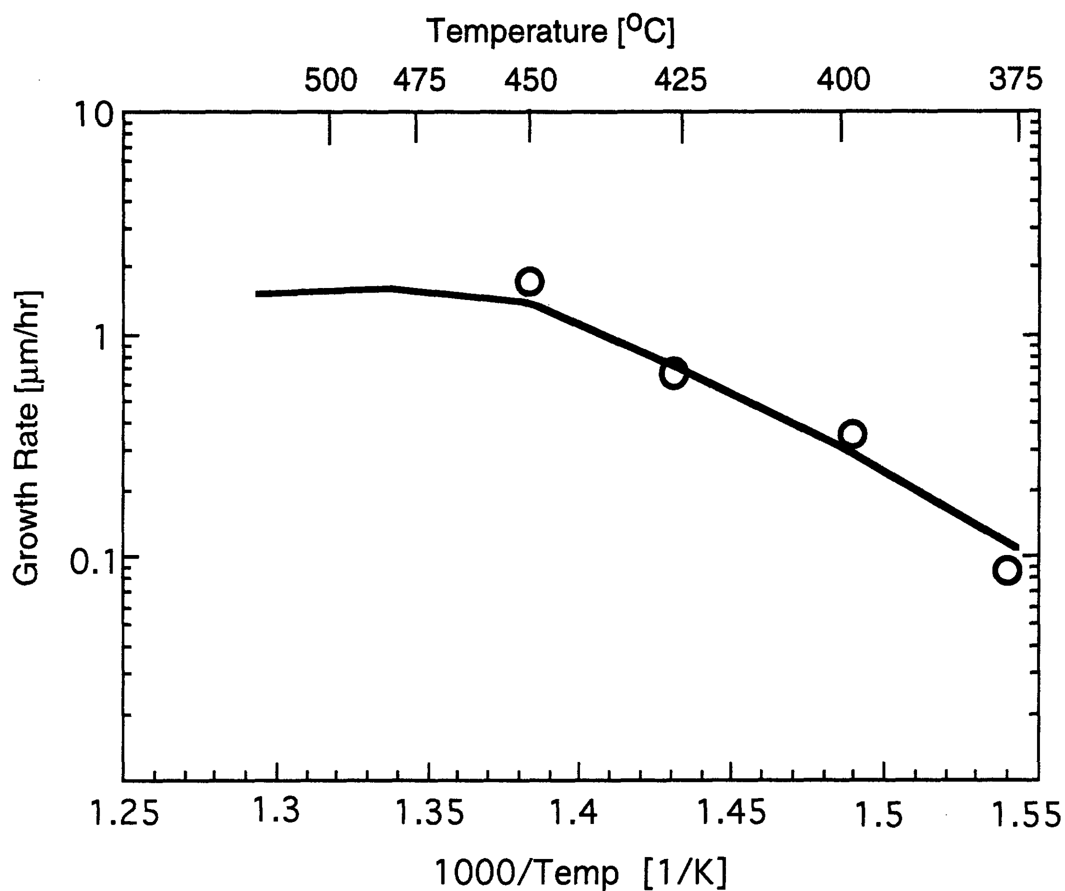

Figure 4.4: Comparison of ZnSe growth rates measured during a single growth experiment (——) and individual growth experiments (**O**). All growth experiments were in He with TPPSe (5 µmol/min) and DMZn (5 µmol/min).

situ laser interferometry measurement is an effective way of planning future growth experiments.

Surface Morphology

Since the surface roughness will affect the amount of scattering of the laser beam, observation of the absolute intensity of the light collected will yield information on the overall surface morphology of the epitaxial film. It should be noted that in all of the growth experiments a general decrease in the intensity of light collected can be observed, as well as a decrease in the difference between the maxima and minima of the light output as the film grows. These trends are consistent with a general degradation in surface morphology as the film grows. Figure 4.5 illustrates the collected light intensity for two growth experiments. By observing the level of the peak maximas in Figure 4.5b, a much more pronounced decrease in the intensity of light collected is seen. SEM micrographs of these films are shown in the insets. The degradation in the surface morphology seen in Figure 4.5b is consistent with the degradation in the light output signal. Thus qualitative information of the surface morphology can be obtained in situ. While these observations were not stressed in the research performed in this thesis, it demonstrates the potential for this technique to provide more than just growth rate measurements. Information on when the surface morphology begins to deteriorate, is something that can not easily be obtained by post growth measurements. In order to detect the beginning of degradation in surface morphology without the benefit of an in situ measurement technique, it would be necessary to perform numerous growth experiments of varying film thickness. Additionally, it is believed that through careful monitoring and positioning of the laser beam, some quantitative information may be obtained by measurement of the absolute light intensity. The light intensity output would need to be calibrated with ex situ measurements (atomic force microscopy, scanning electron microscopy) of the surface morphology.

Other Uses

Another area in which the in situ laser interferometry prove to be invaluable was in the detection of problems that cropped up during growth. As noted in the previous chapter, due to the low volatility of the Se precursors, it was necessary to heat all of the delivery lines in order to prevent condensation of the source

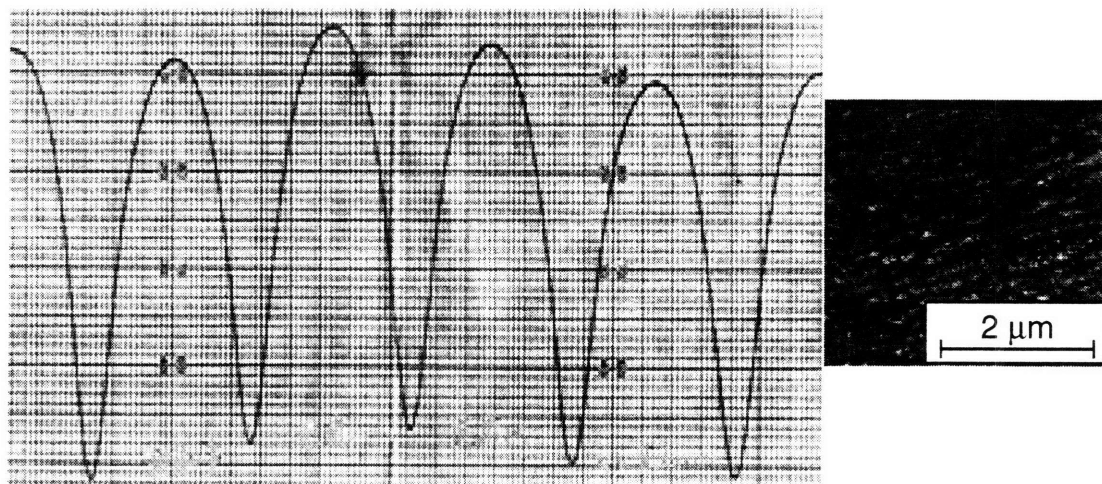

a

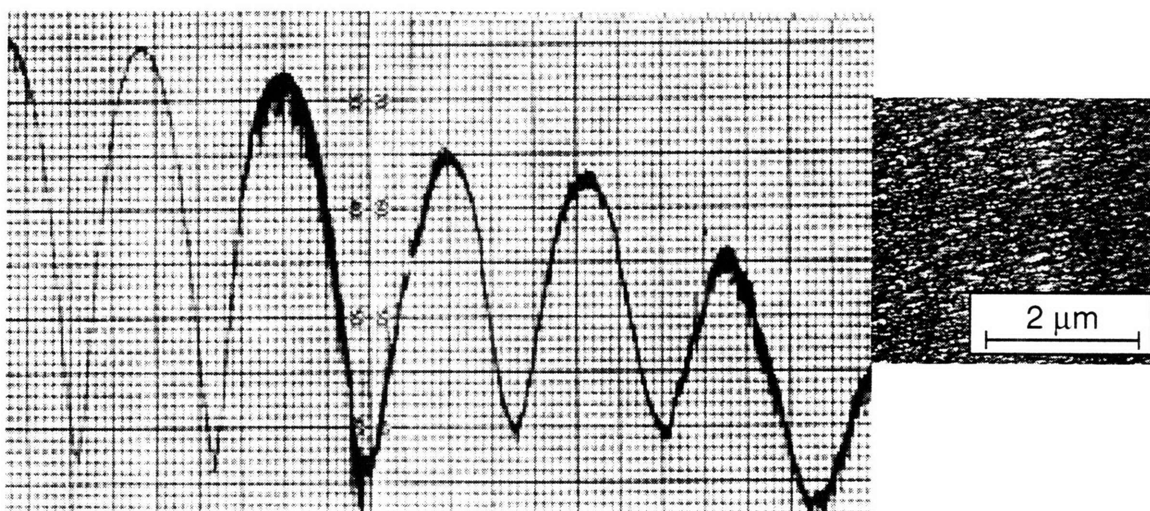

b

Figure 4.5: Laser interferometry output of ZnSe films of varying surface morphology. The output is light intensity as a function of time. The inset is an SEM micrograph of the films.

material. Despite the continuous monitoring of the temperature of the lines, occasionally a cold spot would develop, thereby reducing the delivery rate of the source. This is a problem that could not be easily detected by ex situ measurements and characterization. Since there are many potential problems that could arise during OMVPE growth, an anomaly in the characterization results can not always be easily traced back to a particular problem. However, by monitoring the growth rate of the film in situ, a change in the delivery rate in the Se source was noticed quickly by a decrease in the growth rate of the film. Similarly, exhaustion of a source could be observed in situ by monitoring the light output and the growth experiment could be terminated. The ability to detect problems during growth proved quite valuable in saving both time and source material.

Limitations

While the laser interferometry proved to be invaluable for ZnSe epitaxial growth, there are some limitations of this technique. While this technique has the advantage of performing several measurements during a particular growth experiment, and is quite useful in establishing a rough operating window, it only provided information on the growth rate and qualitative information on the surface morphology; it was still necessary to perform individual growth runs in order to fully characterize the effect of operating conditions on the films. Furthermore, compatibility with the reactor is also an issue. Although the experimental equipment and setup is relatively simple, a means of getting the light in and out of the reactor is necessary. This was easily done in the vertical reactor used in this thesis, but may become more difficult with other reactors, such as the horizontal setup. Finally, the use of this technique is limited by the materials system being investigated. The incident light must be transparent to the epitaxial film grown, thus for smaller bang gap material systems, longer wavelength lasers and detectors are required. Furthermore, the substrate material must be opaque to the incident radiation. This is needed in order to get the reflection of light at the epitaxial film-substrate interface which causes the interference with the reflection of light at the air-epitaxial film interface. In many growth systems, the epitaxial film and substrate film are the same material and this technique can not be used. It is for this reason that reflection and scattering of light at the surface was investigated for potential in situ applications in the growth of other semiconducting materials. These investigations will be detailed in the following sections.

4.2 Laser Light Scattering of Sb-based Films

4.2.1 Experimental Setup

A significant advantage of utilizing the laser light scattering technique is the relative simplicity of the experimental equipment. A 5 mW He-Ne laser was used in conjunction with a silicon photodetector. The experimental setup for the specular reflectance studies is shown in Figure 4.6a. A rotating stage was utilized so that it would be possible to investigate the effect of the orientation of defects on the intensity of light collected. For the experiments investigating the effect of the angle of incidence, care was taken to keep the distance of the laser to the film and the film to the photodetector consistent. Furthermore, the reflected beam was kept normal to the surface of the photodetector. Typical intensities varied from 25-70 mV and were measured with a digital voltmeter. Films of various surface morphology, ranging from excellent, smooth morphologies to poor, high defect density morphologies were studied. Details on the growth conditions of the epitaxial films investigated will be discussed as the results are presented.

The investigation of the diffuse scattering utilized a similar setup (Figure 4.6b) with the exception of the placement of the photodetector. The photodetector was placed directly above the sample and it was necessary to place the photodetector very close to the films (~ 1 cm) in order to insure that an appreciable signal could be measured. Typical intensities varied from 0.05 mV to 10 mV, depending on the surface morphology of the films.

4.2.2 Specular Reflection

The specular reflection of InGaAsSb films that were previously grown was initially studied. Measurements were performed in order to establish the optimal setup, along with identifying the sensitivity and type of information that can be obtained by this technique. The GaSb and InGaAsSb films were grown in a vertical, downward flow reactor. A H_2 carrier gas with a flow rate of 10 liters/min was utilized and the precursors were trimethyl indium, triethyl gallium, tritertiarybutyl arsenic, and trimethyl antimony. The films were chosen to give a range of

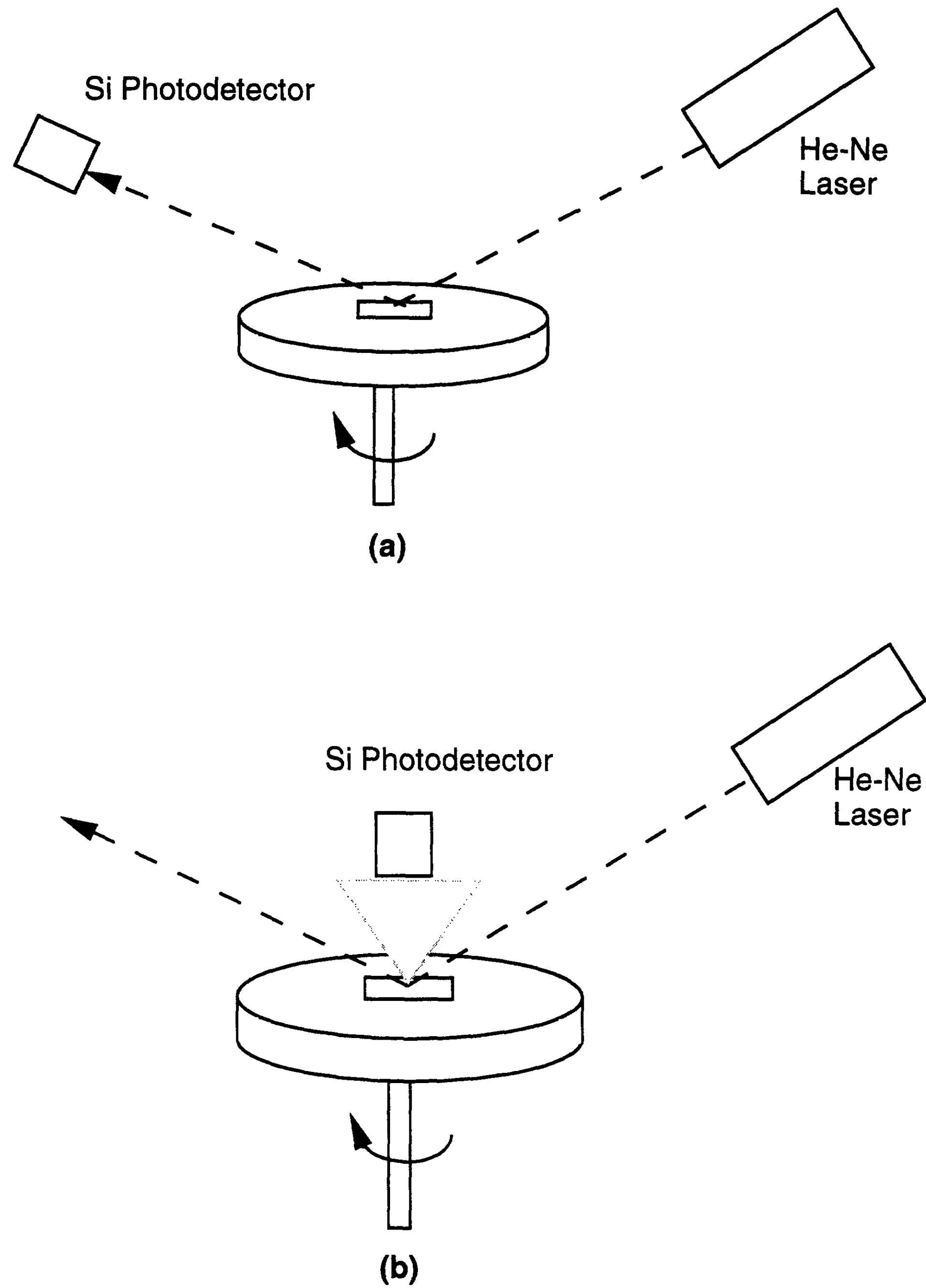

Figure 4.6 : Schematic of experimental setup for laser light scattering for (a) specular reflection and (b) diffuse scattering.

surface morphologies varying from excellent, mirror films, to poor, defect concentrated morphologies.

Effect of Incidence Angle

The effect of the angle of incidence on the specular reflection was first explored in order to obtain a clearer picture of the optimal geometric setup, as well as to obtain an idea of the sensitivity of this technique. The specular reflection intensity as a function of angle of laser light incidence from the normal is plotted in Figure 4.7. The InGaAsSb films were chosen to represent a range of surface morphologies and optical photographs of these films are illustrated in Figure 4.8.

As seen in Figure 4.7, there is a general increase in intensity as the incidence angle is increased away from the normal, however the ability to distinguish between the various surface morphologies decreases. Films A and B, which had very similar surface morphologies, had similar specular beam intensities. Film C was characterized by an orange peel texture, and had lower specular beam intensities, but the intensity was found to increase more rapidly as shallower angles were approached. Film D was also characterized by an 'orange peel' texture, but had a much higher concentration of defects on the surface. This film had the lowest specular beam intensity, however it also was the most sensitive to the angle of incidence. While for an in situ application, high specular intensities are desired in order to more easily obtain a strong signal, there is a marked decrease in the sensitivity of this technique to distinguish between excellent and poor morphology samples. An angle closer to the normal is desired since as the angle approaches normal, the ability to distinguish between various surface morphologies is maximized. However, the compatibility to the particular reactor must be considered; since there is a metal endcap on the top of the reactor it would be necessary to have optical windows inserted in the end cap. The particular reactor used for the growth of these samples would require three optical windows in the cap, and thus the loss of intensity from reflection off of the windows is another important consideration. A more careful look at Figure 4.7 shows that there remains a large difference in intensities up to an angle of approximately 50-60 degrees from the normal. Since the walls of the reactor are quartz, it is possible to use this configuration. Measurement of film B in the reactor at these angles, exhibited a specular reflection intensity of 15 mV, approximately a 75% reduction of the signal

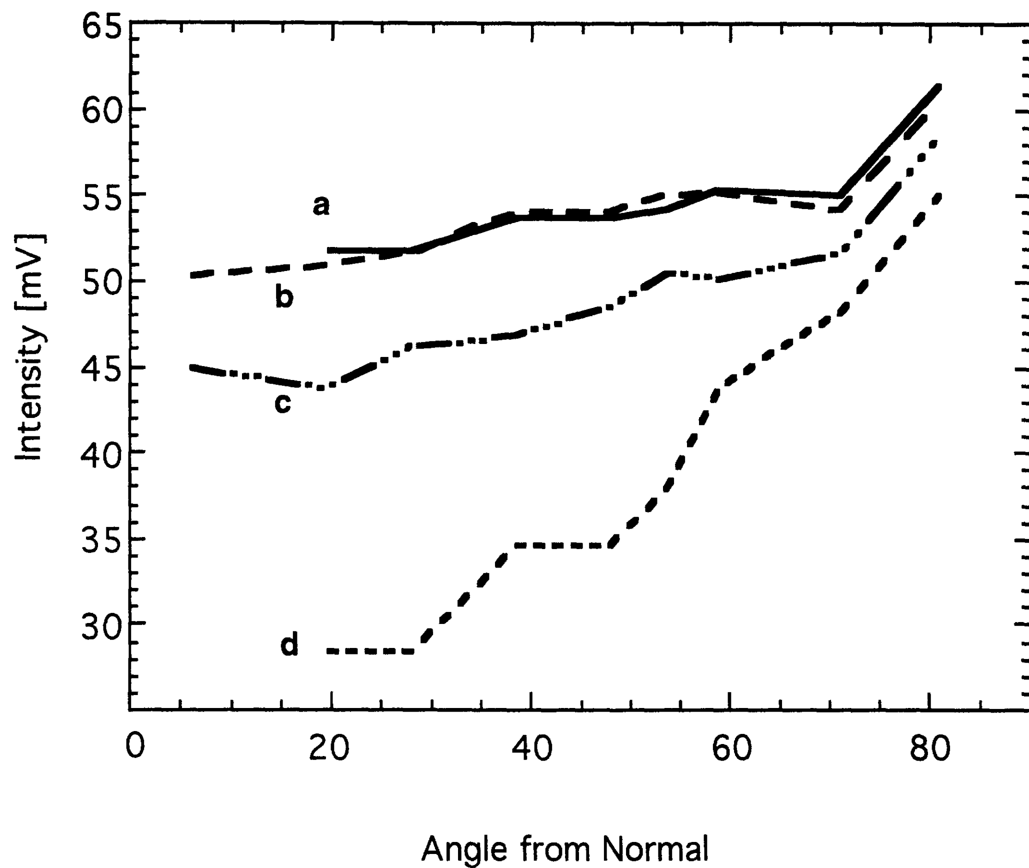

Figure 4.7: Variation of specular beam intensity as a function of angle of incidence for four InGaAsSb films of vaying surface morphology. Images of the four films can be seen in Figure 4.8.

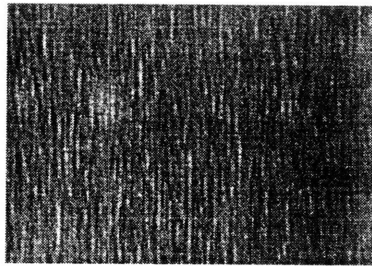

a

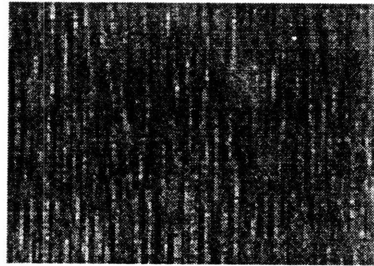

b

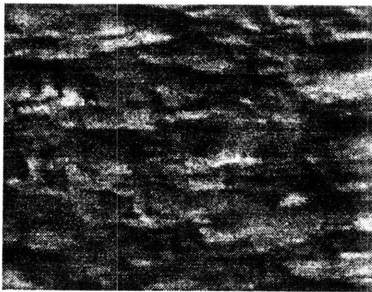

c

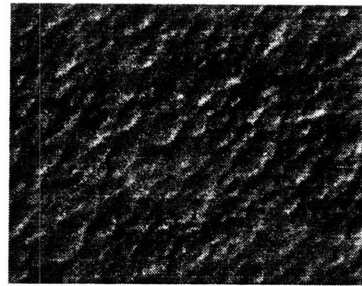

d

Figure 4.8: Normarski phase contrast images of the four InGaAsSb films investigated in Figure 4.7. The images were taken at a magnification of 1600X.

from interactions of the light with the quartz walls of the reactor. While this is a significant loss of signal, it was still easily measured.

Effect of Orientation of Defects

Information on the types of defects on the surface, in addition to the overall morphology of the sample, would be valuable information for an in situ measurement. Thus the sensitivity of the orientation of previously grown films to the incident radiation was explored. Figure 4.9 illustrates the dependence of the specular beam intensity with the orientation of the film along with a Normarski phase contrast image of the film. The arrow next to the film represents the initial point (rotation = 0 degrees) of the radiation. The samples were then rotated in steps of 45 degrees in a counterclockwise direction while the intensity of the collected light was monitored. The film with the smooth, mirror morphology, exhibited no dependence of the specular reflection on the orientation of the film. This is consistent with the surface morphology since the light will be incident on a similar section of the film, regardless of the orientation. Similarly, the film with the poor morphology exhibited no sensitivity to orientation of the pyramidal defects. This is somewhat unexpected since the scattering of the film should change as the orientation of the defect, and the surface that the light scatters from, changes as the sample is rotated. This would suggest that this technique is rather insensitive to the particular geometry of the defect. The insensitivity of the specular reflection technique to the particular defects on the surface led to the investigation of another technique, the study of diffuse scattering.

4.2.3 Diffuse Scattering

Similar to the study of specular reflectance, a variety of previously grown samples ranging in surface morphology from excellent to poor were explored in order to determine the potential of this technique. Due to the low intensities of the scattered light off of the mirror sample , the photodetector was placed very close to the samples (1 cm), and thus it was only possible to explore the shallower angles of incidence on the samples.

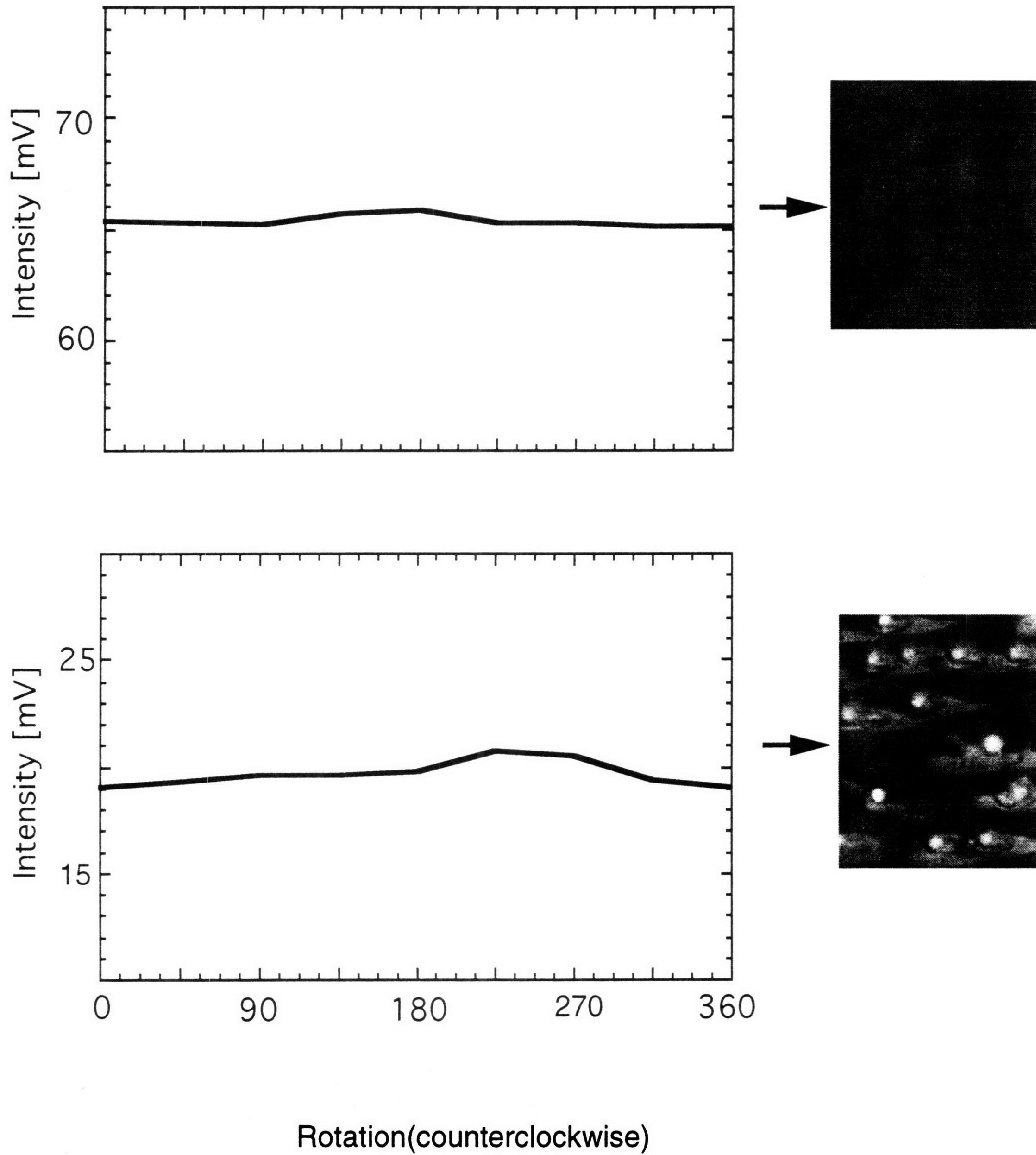

Figure 4.9: Variation of specular beam intensity as a function of the orientation of the surface morphology for two GaSb films. The images are Normarski phase contrast images of the surface morphology, with the arrow indicating the intial incidence (Rotation = 0) of the laser beam.

Effect of Orientation of Defects

As in the study of the specular reflectance, the samples were rotated as the effect of the orientation of the light on the sample was explored. Figure 4.10 illustrates the dependence of the intensity of the diffuse scattering on the orientation of the film. The images in the figure are Normarski phase contrast photographs of the surface of the samples, and once again the initial orientation of the light on the sample is indicated by the arrow. Film A, which had a smooth surface morphology, was found to exhibit no orientational dependence of the diffuse scattering. However, films B and C both exhibited an orientational dependence of the defects on the amount of diffuse scattering. Both films had maximas in the diffuse scattering when the laser light was incident perpendicular to the long axis of the defects, while there was a minimum when the light was incident normal to the shorter axis. When the light is incident normal to the long axis of the defect it is exposed to a larger area of the defect, which will result in an increase in the intensity of the diffuse scattering. Furthermore, the significant difference in the measured intensities of the diffuse scattering should be noted. Film A, with the excellent morphology, had an intensity of approximately 0.05 mV while there is an increase of nearly two orders of magnitude when films B and C are observed, indicating the sensitivity of this technique to both the overall surface morphology and the orientation of the defects on the surface. Finally, information on the concentration of defects on the surface may also be obtained from this technique. Films B and C both contain similar defects on the surface, but have different defect densities. The intensity of diffuse scattering from film B is approximately 33% of the intensity of film C. Thus it may also be possible to correlate the defect density to the diffuse scattering intensity if the defect is known.

Limitations

The major limitation of this technique is the compatibility to the experimental equipment. The measurements for this technique were made by placing the photodetector 1 cm away from the sample; this is not possible for an in situ setup, and an alternative configuration must be found. It would appear difficult to simply focus the diffuse scattering to the photodetector. This would require an optical window in the end cap on the reactor, and based on the distance between the sample and the lens dictated by the size of the reactor, and the relatively small

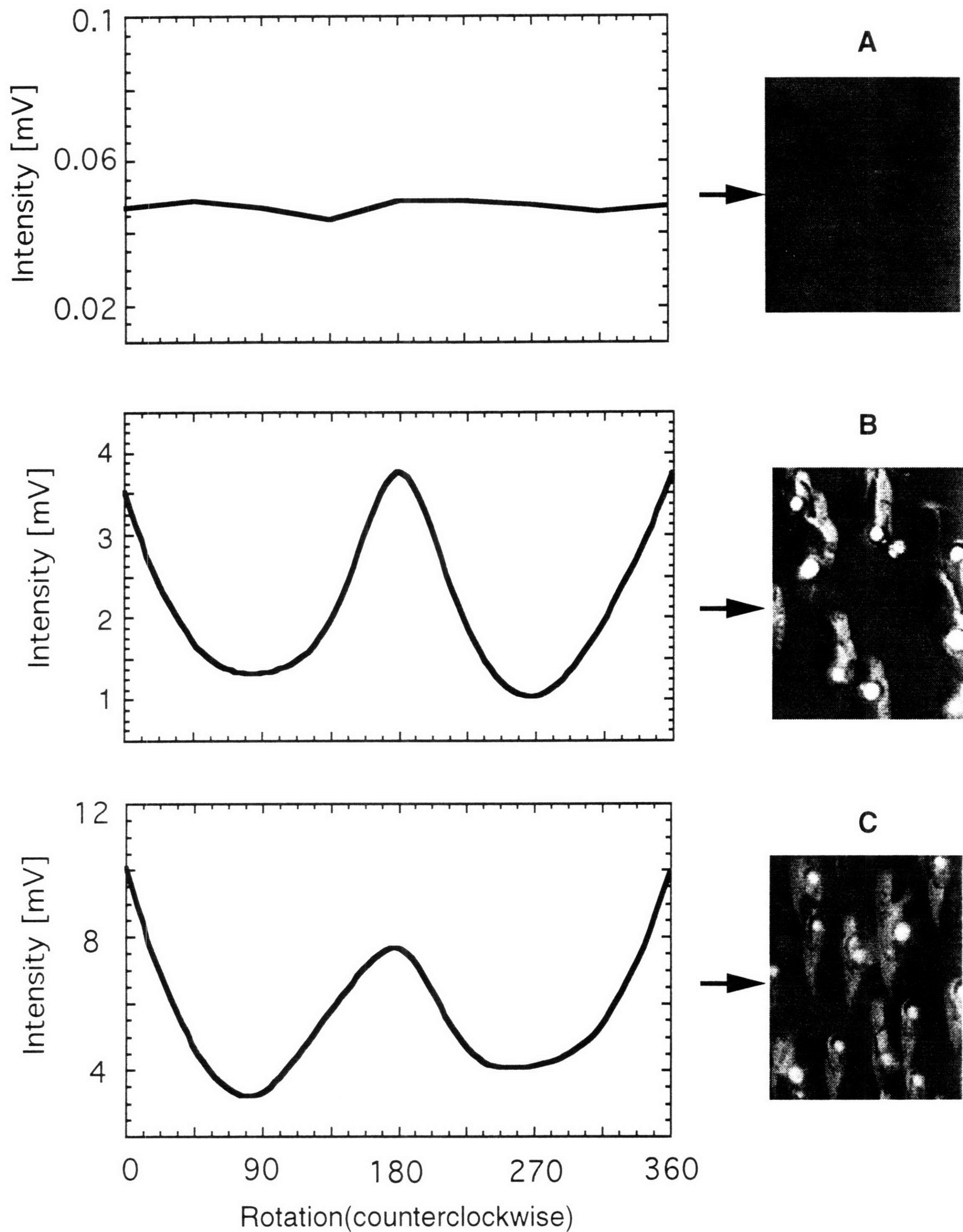

Figure 4.10: Diffuse scattering as a function of orientation for GaSb films of varying surface morphology. The arrow indicates the initial position of the incident light (Rotation=0) with respect to the surface morphology. The Normarski phase contrast images represent a magnification of 1600X.

collection area available, it would appear that an in situ measurement could not be performed with a simple photodetector. Some means of amplifying the light signal is necessary.

5 Conclusions

5.1 ZnSe Growth

OMVPE growth of ZnSe from tri-n-propyl phosphine selenide and dimethyl zinc in a He carrier gas produced high quality epitaxial films. Under deposition temperatures ranging from 375-450 ^{o}C, growth rates on the order of 0.5-1.5 μm/hr were obtained. The films were characterized by an 'orange peel' surface morphology and exhibited strong excitonic emission, with little deep level emission. SIMS analysis revealed low levels of H, C, and P incorporation, indicating the potential of phosphine selenide compounds for p-type OMVPE ZnSe applications. Growth of ZnSe films in H_2 carrier gas revealed a change in the growth chemistry. SIMS profiles showed dramatic increases in the H and P incorporation levels and the growth rate increased by nearly an order of magnitude. Similarly the PL showed a significant increase in deep level emission.

Since the TPPSe has a vapor pressure that is too low for practical OMVPE applications, alternative phosphine selenides were explored. The investigation of an alternative phosphine selenide, DMBPSe, yielded an increase of nearly an order of magnitude in vapor pressure, with similar growth results. Further exploration for a higher volatility phosphine selenide that may be utilized at room temperature is necessary.

The presence of donor bound exciton and donor acceptor pair peaks in the PL spectra reveal the probability of Cl contamination of the Se sources. Purification of the phosphine selenide sources will be necessary to achieve higher quality, non-

compensated p-type material. Increased levels of H, C, and P atoms at the surface and ZnSe/GaAs interface demonstrates a need for an alternative pretreatment step to the phosphine selenide passivation. Similarly, exposure to the phosphine selenide during the cool down must be avoided.

Investigations of TMSAZ as a potential nitrogen doping source was explored. Based upon the dramatic increase in the growth rate and increased levels of deep level emission in the PL spectra, it is believed that the growth chemistry of the phosphine selenides was altered by the presence of this compound. While growth using lower delivery rates of this source by setting up dilution lines on the OMVPE system may be explored, based upon previous investigations of this source with H_2Se and DMZn, it is believed that there is limited potential for the compatibility of this doping source with the trialkyl phosphine precursors.

5.2 ZnSe Laser Interferometry

The in situ laser interferometry proved to be a very useful tool for the growth of ZnSe. Comparison of the in situ thickness measurements with SEM analysis demonstrated the interferometry technique to be highly accurate. Observation of the absolute intensity as well as the difference between the minima and maxima in the intensity of the reflected beam provided qualitative information on the surface roughness of the samples. This technique also proved to be invaluable in establishing a rough operating window for determining future growth experiments for variables such as VI/II ratio and growth temperature. The ability to measure several growth conditions in a single growth experiment saved both time and source materials. This technique also proved to be highly beneficial in trouble shooting problems that cropped up during growth. While this technique was quite valuable for ZnSe growth, it is limited by the materials system being investigated.

The incident light must be transparent to the epitaxial film grown, while opaque to the substrate.

5.3 Laser Light Scattering

Two different laser light scattering technique were explored for their potential as in situ measurement techniques. While the specular reflectance measurement had the advantage of experimental simplicity, it was found to be quite limited in the measurement of surface roughness, and was insensitive to the orientation of defects on the surface. Although this technique did provide some qualitative information on the overall surface roughness of a particular sample, it is believed to be not sensitive enough for useful applications.

The investigation of the diffuse scattering off of epitaxial films appeared to show more promise for potential in situ applications. This technique was quite sensitive to the overall surface morphology of the films investigated, as well as to the orientation of the defects on the surface. However, there are some potential obstacles in the compatibility with OMVPE reactors. The intensity of the diffuse scattering was found to be quite low, and there may be problems in obtaining an appreciable signal. Some method of magnifying the light that is compatible with the existing OMVPE reactors is necessary if this technique is to be utilized for in situ applications.

References

[1] J.D. Walker, K. Malloy, S. Wang, and J.S. Smith, *Applied Physics Letters*, **56** (1990) 2493.

[2] K. Okhawa, T. Mitsuyu, and O. Yamazaki, *Extended Abstracts 18th International Conference on Solid State Devices and Material, Tokyo*, (1986) 635.

[3] R.M. Park, M. B. Troffer, C.M. Rouleau, J.M. Depuydt, and M.A Haase, *Applied Physics Letters* , **57** (1990) 2127.

[4] M.A. Haase, J. Qiu, J.M. Depuydt and H. Cheng, *Applied Physics Letters*, **59** (1991) 1272.

[5] W. Xie, D.C. Grillo, R.L. Gunsher, M. Kubayashi, G.C. Hua, N. Otsuka, H.Jeon, J. Ding, and D.V. Nurmikko, *Applied Physics Letters*, **60** (1992) 463.

[6] H. Jeon, J. Ding, W. Patterson, D.V. Nurmikko, W. Xie, D.C. Grillo, M. Kobayashi and R.L. Gunsher, *Applied Physics Letters*, **59** (1991) 259.

[7] S. Sritharan, K.A. Jones, and K.M. Motyl, *J. Crystal Growth*, **68** (1984) 656.

[8] K.P. Giapis, D.C. Lu, and K.F. Jensen, *Applied Physics Letters*, **54** (1989) 353.

[9] A.C. Jones, P.J. Wright, and B. Cockayne, *J. Crystal Growth*, **107** (1991) 297.

[10] H. Mitsuhashi, I. Mitsuishi, M. Mizuta, H. Kukimoto, *Japanese Jounal of Applied Physics*, **24** (1985) L578.

[11] G.B. Stringfellow, *J.. Electronic Materials*, **17** (1988) 327.

[12] R. Korenstein, W.F. Hoke, P.J. Lamonias, and S.J. Pachuta, *J. Applied Physics*, **62** (1987) 4929.

[13] K.P. Giapis, K.F. Jensen, J.E. Potts, and S.J. Pachuta, *Applied Physics Letters*, **55** (1989) 463.

[14] W. Kuhn, R. Driad, H. Stanzl, A. Lusson, K. Wolf, B. Qu'Hen, H. Sahin, L. Svob, C. Grattepain, X. Quesada, W. Gebhardt, O. Gorochov, *J. Crystal Growth*, **138** (1994) 448.

[15] A. Kamata, T. Uemoto, M. Okajima, K. Hirahara, M. Kawachi, T. Beppu, *J. Crystal Growth*, **86** (1988) 285.

[16] B.J. Skromme, M.C. Tamargo, J.L. de Miguel, and R.F. Hahory, *Materials Research Symposium Proceedings*, **102** (1988) 577.

[17] H. Cheng, J.M. Depuydt, J.E. Potts, and M.A. Haase, *J. Crystal Growth*, **95** (1989) 512.

[18] N. Shibata, A.Ohki, and A. Katsui, *J. Crystal Growth*, **93** (1988) 487.

[19] M.A. Haase, H. Cheng, J.M. Depuydt, and J.E. Potts, *J. Applied Physics*, **67** (1990) 448.

[20] H. Cheng, J.M. Depuydt, J.E. Potts, and T.L. Smith, *Applied Physics Letters*, **52** (1987) 147.

[21] K. Kosai, B.J. Fitzpatrick, H.G. Grimmeis, R.N. Bhargava, and G.P. Neumark, *J. Cryt\stal Growth*, **91** (1988) 639.

[22] T. Yao and Y. Okada, *Japanese Journal of Applied Physics*, **25** (1986) 821.

[23] H. Jeon, J. Ding, A.V. Nurmiko, W. Xie, and D.C. Grillo, *Applied Physics Letters*, **60** (1992) 2045.

[24] N.R. Taskar, B.A. Kahn, D.R. Dormen, and K. Shahzad, *Applied Physics Letters*, **27** (1988) 2195.

[25] J.A. Wolk, J.W. Ager III, J.K. Dugasted, E.E. Haller, N.E. Tasker, D.R. Norman, D.J. Olego, *Applied Physics Letters*, **63** (1993) 2756.

[26] A. Kamata, H. Mitsuhashi, and H. Fujita, *Applied Physics Letters*, **63** (1993) 3353.

[27] J. Huh, S. Patnaik, and K. Jensen, *J. Electronic Materials*, **22** (1993) 509.

[28] P.J. Dean, D.C. Herbert, C.J. Werhoven, B.J. Fitzpatrick, and R.N. Bhargava, *Physics Review B*, **23** (1981) 4888.

[29] A.J. Springthorpe and A. Majeed, *J. Vacuum Science Technology B*, **8** (1990) 266.

[30] T. Farrell, J.V. Armstrong, and P. Kightley, *Applied Physics Letters*, **59** (1991) 1203.

[31] H. Sankur, W. Southwell and R. Hall, *J. Electronic Materials*, **20** (1991) 1099.

[32] N.C. Frateschi, S.G. Hummel, and P.D. Dapkus, *Electronic Letters*, **27** (1991) 155.

[33] T. Makimoto, Y. Yamaguchi, N. Kobayashi, and Y. Horikoshi, *Japanese Journal of Appliied Physics*, **29** (1990) L207.

[34] J.M. Olson and A. Kibbler, *J.Crystal Growth*, **77** (1986) 182.

[35] D.E. Aspenes, W.E. Quinn, and S.Gregory, *Applied Physics Letters*, **56** (1990) 2569.

[36] W.E. Quinn, D.E. Aspenes and S. Gregory, *J. Crystal Growth,* **107** (1991) 1045.

[37] Y. Horikoshi, H. Yamaguchi, F. Briones, and M. Kawashima, *J. Crystal Growth,* **105** (1990) 326.

[38] A.J. Pidduck, D.J. Robbins, A.G. Cullis, D.B. Gasson and J.L. Glasper, *J Eletrochemical Society,* **136** (1989) 3083.

[39] A.J. Pidduck, D.J. Robbins, A.G. Cullis, D.B. Gasson and J.L. Glasper, *J Electrochemical Society* , **136** (1989) 3088.

[41] H. Burger, D. Sawodny, and W. Wannagat, *J. Organometallic Chemistry,* **23** (1984) 1972.

[42] W.S. Rees Jr, and D.M. Green, *J. Electronic Materials,* **21** (1992) 361.

[43] J. E. Potts, H. Cheng, S. Mahapatra and T.L. Smith, *J. Applied Physics,* **61** (1987) 333.

[44] B.J. Skromme, M.C. Tamargo, F.S. Turco, S.M. Shibli, W.A. Bonner, and R.E. Nahory, *GaAs and Related Compounds, Atlanta, 1988, Inst. Phys. Conf. Ser. 96, Ed. J.S. Harris (Inst. Phys., Bristol, 1989)* 205.

[45] T. Yao, Y. Okada, S. Matsui, K. Ishida and I. Fujimoto, *J. Crystal Growth,* **81** (1987) 518.

[46] A. Yoshikawa, S. Muto, S. Yamaga, H. Kasai, *J Crystal Growth,* **93** (1988) 697.

[47] H. Mitsuhashi, I. Mitsuishi, M.Mizuta and H. Kukimoto, *Japanese Journal of Applied Physics,* **24** (1985) 2256.

[48] W. Stutius, *Applied Physics Letters,* **40** (1992) 246.

[49] K. Nishimura, Y . Nagao, K. Sakai, *Japanese Journal of Applied Physics,* **32** (1993) L 428.

[50] K. Nishimura, Y. Nagao, K. Sakai, *J Crystal Growth,* **134** (1993) 293.

[51] J.L. Merz, K. Nassau, and J.W. Shiever, *Physics Review B,* **8** (1973) 1444.

[52] M. Heuken, *J Crystal Growth,* **146** (1995) 570.

[53] T. Yodo, and K. Yamoshita, *J. Crystal Growth,* **93** (1988) 656.

[54] Y. Zhang, W. Liu, B.J. Skromme, H. Cheng, S.M. Shibili, and M.C. Tamargo, *J. Crystal Growth,* **138** (1994) 310.

[55] J. Gutowski, N. Presser and G. Kudiek, *Physical Status Solidi*, **120** (1990) 11.

[56] K. Shahzad, D. Olego, and D.A. Cammack, *Physics Review B*, **39** (1989) 1306.

[57] M.Danek, J.S. Huh, L. Foley, and K.F. Jensen, *J. Crystal Growth*, **145** (1994) 530.

[58] K. Wolf, H. Stanzl, A. Naumov, H.P. Wagner, W. Kuhn, B. Hahn, W. Gebhardt, *J. Crystal Growth*, **138** (1994) 412.

[59] B.J. Skromme, W.Liu, K.F. Jensen, K.P. Giapis, *J. Crystal Growth*, **138** (1994) 338.

[60] D.J. Stachan, M.Mingila, M.C. Tamargo, and B.A. Weinstein, *J. Crystal Growth*, **138** (1994) 318.

[61] K.P. Giapis, D.C. Lu, K.F. Jensen, and J.E. Potts, *J. Crystal Growth*, **104** (1990) 291.